A THESIS FOR THE DEGREE OF DOCTOR OF PHILOSOPHY

Design and Fabrication of Soft Sensors for Wearable Electronics and Robotics Applications

Afaque Manzoor

Department of Mechatronics Engineering

GRADUATE SCHOOL

JEJU NATIONAL UNIVERSITY

2021. 02

Design and Fabrication of Soft Sensors for Wearable Electronics and Robotics Applications

Afaque Manzoor

(Supervised by Professor Kyung Hyun Choi)

A thesis submitted in partial fulfillment of the requirement for the degree of Doctor of Philosophy

2021. 02

The thesis has been examined and approved.

.....

Thesis Director: Jong-Hwan Lim, Professor, Department of Mechatronics Engineering

.....

Supervisor: Kyung Hyun Choi, Professor, Department of Mechatronics Engineering

.....

Chul Uoong Kang, Professor, Department of Mechatronics Engineering

.....

Chang-Nam Kang, Professor, Department of Mechanical Engineering

.....

Myung taek Hyun, Professor, Department of Mechanical Engineering

.....

Date

Department of Mechatronics Engineering

GRADUATE SCHOOL
JEJU NATIONAL UNIVERSITY
REPUBLIC OF KOREA

To my mother, who made me what I am today.

Acknowledgements

I want to start my acknowledgement from the sentence I always proudly say, 'Ami, Whatever I am today, is only because of you!'. My all praise, love, prayers to my mother who showered her unconditional and continuous blessings upon me with strength, courage, and knowledge; and helping me out constantly to achieve this honor. While continuously giving my best during long journey of PhD, the only thing that kept me motivated is one sentence that my late mother used to say every time; 'Kujh bhi the, man pahinje mithan khe parhaeendas' (sindhi sentence, translation: I will do everything to get my mithan (she used to call me with this name often) educated). She always dreamed to see me at a place where my whole family could feel proud at. And yes, I can say today, I have significantly achieved what my she imagined. In fact, her training, untiring efforts, and never-ending love even in the worst days of her life enabled me to do something which is exception in my own capacity. She always kept me with her, I never ever thought to leave my country for even a week. In fact, She used to cry, even if I left home for day on business trip. Rest in power, Ami !

My sincerest gratitude also goes to my late father who left this world back in 2002. But his sincere efforts in teaching social services have always been with me as driving force to contribute to society to the best of my abilities. I would also like to thank my sisters and brother; Hina, Riffat, and Tarique; and my fiancée Mahira, Bhabhi Aliza whose support was always there when I needed it the most. In fact, the major credit of this degree directly goes to them. The time I used to get upset, I used to talk to hassan, Tehreem and Moutar (my nephew and twin nieces). Their happy and mischievous faces used to bring never-ending happiness to my life. I am waiting for the day, when these kids will read this and I am sure they will feel proud. I am also highly indebted to Mama Imtiaz, Tarique Manzoor and Bhaijan Zubair; their contribution to my career development is exceptional. I will end up with the words but will not be able to write for them.

I am extremely thankful to Prof. Kyung Hyun Choi who is the best PhD supervisor I could have asked for. I will always be indebted to him for his kindness, endless support, and guidance throughout my program. I would remember the amount of trust he has put into me and the confidence that I got as

a result. I wish him all the happiness in his life. I would also like to thank all the other teachers in my life; Saen Muhammad Akram (Primary School), Saen late Ali Dost Junejo, Saen Nadeem Shah, and Saen Iftikhar Abro (High School), Saen Abdul Razak Baloch, Saen Mushtaq Ahmed Ansari, Saen Shahid Akhtar Memon, Saen Bansi Lal (College), Dr Madad Ali Shah, Dr Muhammad Waqas, Saen Aziz Altaf, Saen Abid Memon, Saen Mir Muhammad Lodro, Dr Aslam Pervaiz (University) who have been the real builders of my personality and the torchbearers of knowledge for me at each and every stage of my life.

I am thankful to my friends who have played very important role in my life; they include Asif Nawaz Qazi, Suhail Almani, Usman Ahmed, Sunny Katyara, Jamshaid Ansari, Yaseen Shah, Noor Khoso, Noor Nawaz Sethar, Amir Hussain Arain. I am also very happy to mention two exceptionally well souls; Hina Ashraf and Faiza Jabbar. Their contribution to my PhD is beyond words. I am highly indebted to them for everything they have done for me. I am also thankful to all my AMM lab members for their wonderful and continuous support in my research work.

I would take this opportunity to thank the wonderful people of Korea and particularly Jeju who have always been kind to me and other foreigners. Everyone here is very helpful, humble, friendly, honest, and awesome. Living on a small island for four years, thousands of miles away from home, in a different culture with people speaking an unrecognizable language seemed a walk in the park just because of the amazing natives of this great country.

Afaque Manzoor, December 17, 2020

Contents

List of Figures

List of Tables

Abstract

This research work deals with the design and fabrication of fast ultra-flexible sensing devices through state-of-the-art technologies like multi-head 3D fabrication techniques and Reverse Offset Printing. The devices like soft sensors (strain and humidity sensors) have been developed with successful target of enhancing the features like sensing capacity, detection range, detection limit, cyclic stability, hysteresis, data reproducibility and accuracy. These milestones were significantly attained through articulated cutting-edge research of selection of active material and its relevant synthesis, device structure optimization through simulation and working principle and implementation of device using compatible fabrication system. Two strain sensing devices were fabricated based on the novel conductive materials, Gly-KCL and PEDOT: PSS/MWCNTS after a fully optimized sensor' design using FEA tool of COMSOL 5.4. The developed strain sensors outperformed not only in terrestrial robotic and human motion monitoring but also under aquatic environment due to its water-proof design structure. Moreover, an environmental sensor based on humidity sensing device has also been developed which has prime features of biocompatibility due to active layer of Polylactic-co-glycolic acid (PLGA), all printed fabrication approach, full range responsive sensors (0%- 100%), highly linear and a portable wi-fi enabled interactive system for sensor's response readout. For the characterization of devices, custom-made setups with precise electronic controllers have been developed. The developed sensors have been compared with the commercial as well as reported devices in literature and their results showed them strong candidates to commercially available sensors. In the end, a soft robot mimicking real frog has been modelled and fabricated based on ultra-flexible 3D printable Shape Memory Polymer (SMP) composite filament and shape memory alloy (SMA). After careful mathematical modelling, simulation-based optimization, the developed robot was able to achieve under water synchronous swimming with acceptable thrust force and the adoptability to swim under different applied frequencies using an interactive GUI of LabVIEW controlled custom-made setup. In other words, this research work effectively presents the logical combination of multiple fields of study to fabricate soft sensors with focus on wearable and robotics applications.

1 Introduction

Recently, the soft sensors have gained enormous attention due to their myriad applications such as wearable electronics, personal health monitoring, medical devices, prostheses, smart clothes, and soft robotics. These devices are preferred owing to their characteristics such as high compliance, long lifetime, low weight, and low cost. However, conventional devices contain rigid electronic components which limit their use in human-centric applications and reachability for robots. In fact, soft flexible sensors play a vital role in various fields like motion-feedback for fabricated robots, human health monitoring, electronic skin and flexible touch screens. Unlike soft sensors, conventional sensors use a well-established technology by mainly exploring different forms of buckling, mesh, interlocking, foams and films in carbon and graphene. Ideal sensor should possess characteristics such as highly sensitive, cost-effective, highly specific, have wide operation range, accurate robust, have fast transient response, easy to operate, simple readout circuitry and stable. Moreover, it is practically not possible to achieve all the mentioned features in one sensing device. Rather, there is always some trade-off among those characteristics. In case of application specific sensors, only few qualities are required. Researchers have managed to achieve such goals by using various techniques like device structure, working mechanism, using specific material and fabrication process. Many researchers have developed sensors for targeted applications by just focusing on a single parameter. Like specialized groups in chemistry mainly design the sensors using novel high-performance materials, physicists explore this field by focusing on device structure and its working mechanism, and so on. Recently, the advancement in 3D printing and additive manufacturing has brought new avenues in sensor fabrication in addition to their mass production, which was hardly possible using conventional approaches. 3D printing brings liberty in the design and specifications and enable effective fabrication of complex sensors, memristors, transistors and actuators. Environmental monitoring is crucial for investigating climate change, weather forecasting, health care, industry, and other applications. Parameters like strain, temperature, humidity, radiation, wind speed, gases, light intensity, contamination, etc. are detected both quantitatively and qualitatively to establish a complete set of information. The major parameters used for basic weather monitoring include relative humidity and

temperature. All these factors are crucial in monitoring and control of application-specific environments and health care industry. The devices like ECG electrodes, optical sensors, pressure sensors, tactile sensors, displacement sensors, temperature sensors, chemo/bio sensors, humidity sensors and antennas have been developed using various printing technologies. Novel active electronic materials with required properties to carry out the sensing application have been developed, which have compatibility with additive manufacturing. Further, the working principle of device is thoroughly explored, to optimize the performance parameters. However, it remains unattainable to bring all the parametric features in to one device using mentioned techniques. Using of one specific technique to solve the limitations brings a significant compromise on the complexity of the device structure, performance parameters, cost, fabrication approach, incompatibility with the already available technologies. Therefore, it is evident, that for the development of an ideal sensor for any required application, an articulate knowledge of various fields is indispensable.

To solve these problems, high performance strain and humidity sensors have been developed. Modeling, Fabrication & Control of fast ultra-flexible sensing devices through state-of-the-art technologies 3D printing and Reverse Offset Printing have been achieved. The devices like soft sensors (strain and humidity sensors) have been developed with successful target of enhancing the features like sensing capacity, detection range, detection limit, cyclic stability, hysteresis, data reproducibility and accuracy. These milestones were significantly achieved through articulated cutting-edge research of selection of active material and its relevant synthesis, device structure optimization through simulation and working principle and implementation of device using compatible fabrication system. The main focus has also been to make sure that the manufactured devices possess biocompatibility which is very important when it comes to the device interaction with humans. The fabrication techniques used to develop sensors enable devices to be conformal for wearable electronics applications and robotics applications. The proposed sensors allow simple and seamless integration with the day-to-day gadgets like smart phones.

2 Electronic Materials

2.1 Introduction

For any sort of device fabrication, materials are one of the most vital elements. It is of great importance to select and synthesize appropriate materials based on the required applications[1–3 4–9]. The materials must possess the properties that can perform the desired operation and must also be compatible with the available fabrication technologies that are printing systems in case of this research work. The materials selection and synthesis process start with enlisting the properties required for the target application. Several candidates are short listed based on their intrinsic properties and then one or more of them are selected based on the design and fabrication requirements[10,11]. In current research work targeting environmental and bio-sensing devices, three major categories of materials were studied in detail. They include conductive materials for electrode fabrication, active layer materials for sensing area fabrication, and biomaterials to study the interaction of different bio-reagents and the effects of those interactions. All these materials involved in electronic sensing device fabrication can be referred to as electronic materials due to the change in their electrical properties that can be studied as the device output.

2.2 Electrode Materials

All the sensors fabricated in this research work were based on changes in electronic properties and were listed in the electronic sensor's category. For the fabrication of electronic sensors, a transducer is one of the core device elements that converts any kind of signals into electrical signals that can be detected by the read-out circuits[2,4,5,7–9,11,12]. For the fabrication of the transducers, different conductive inks based on metallic nanoparticles were used. The electrodes were designed in an interdigitated transducer (IDT) pattern. Moreover, for the development of strain sensors, silicon coated electrodes were encapsulated with sensing materials. IDT design was selected based on its superiority in performance relative to other transducer designs owing to its large area and multi chemristors element design. For the humidity sensing devices, silver ink was used as the electrode

material deposited in IDT pattern using Reverse Offset Printing technology. The electrode material and fabrication method were later replaced with silver nano

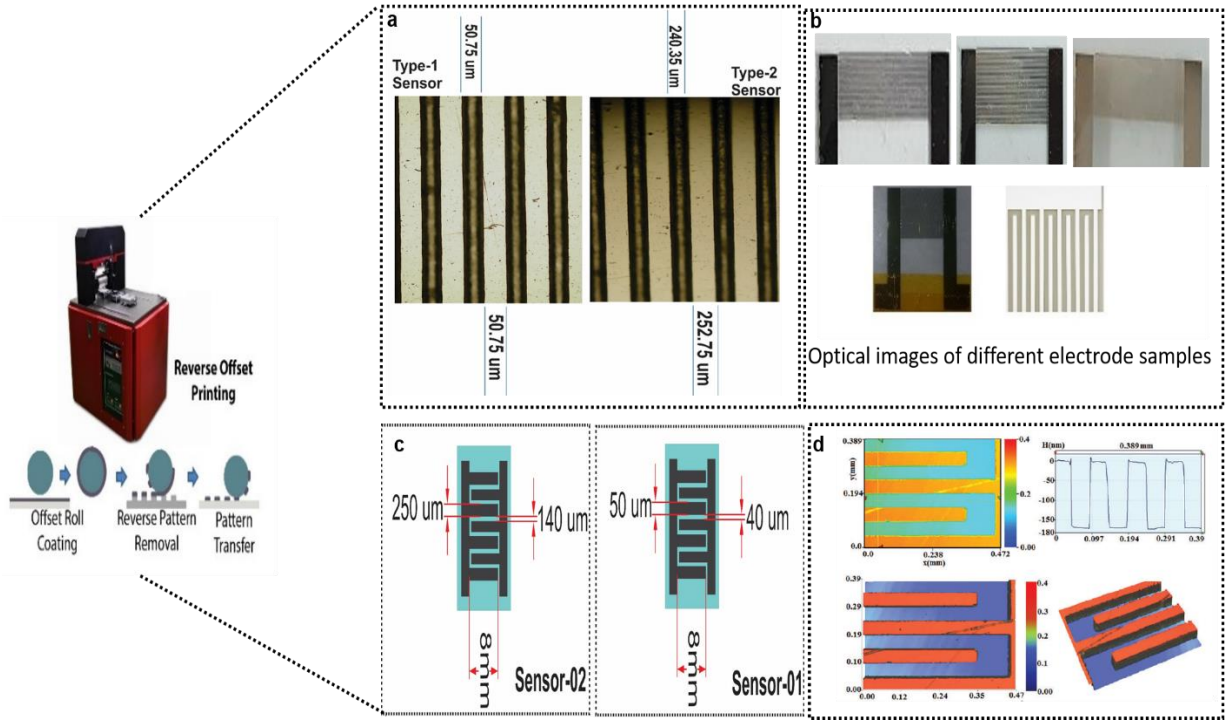

Figure 2-1 a) High magnification images of fabricated electrodes, b) optical images of six different samples of fabricated sensor, c) fabricated sensors' dimensions, d) 3D profile of fabricated electrodes

particle based conductive inks and printing techniques to make it compatible with printed electronic approaches[13]. Two types of commercially available silver nano-particle inks were used for electrode fabrication including Ag nanoparticles ink purchased from PARU with particles diameter range of 20~200 nm, Ag contents of 80~88 wt% and typical resistance of 2.0 mΩ/mil and Silverjet DGH ink for reverse offset (viscosity: 1.5 cps, surface tension: 24.4 mN/m, dispersion matrix: octane based). These inks were compatible with multiple pattern printing systems including reverse offset printing, screen printing, EHD printing, and inkjet printing. However, for initial testing of the sensing mechanism, electronic inks Circuit Scribe Conductive ink pen with ~2 Ω/cm conductivity was used for the hand drawn electrode patterns onto the substrates. The dimensions of designed and fabricated humidity sensors are shown in Figure 2-1.

2.3 Active Layer Materials

Active layer materials possess the highest importance in any electronic sensing device and they are selected after carefully considering their electronic readout capabilities, sensitivity towards the target, saturation values, limits of detection, re-usability, long-term stability, low cost, environmental effects, and so on[13–18]. In this research, a biocompatible Poly lactic glycolic acid (PLGA) is used as a sensing layer for the first time. Moreover, for Strain sensors, A biocompatible composites of glycerol and potassium chloride, and conductive poly(3,4-ethylenedioxythiophene) polystyrene sulfonate multiwall carbon nanotube (PEDOT: PSS/MWCNT[19].

2.3.1 Electronic polymers

The first polymer used for the fabrication of humidity sensors active layer was Poly lactic glycolic acid (PLGA). This is considered as well-known drug delivery polymer. Poly (lactic-co-glycolic acid) is a copolymer of poly (lactic acid) and poly (glycolic acid) which is FDA approved bio compatible and biodegradable polymer which is increasingly used for sustainable drug delivery applications. Poly lactic glycolic acid (PLGA lactic: glycolic =50:50), TFE (2, 2, 2-Trifluoroethanol) and Polyethylene terephthalate (PET) substrate were purchased from Sigma-Aldrich. For the fabrication of silver conductive ink (viscosity: 1.5 cps, surface tension: 24.4 mN/m, dispersion matrix: octane based) was purchased from Silverjet DGH ink for reverse offset printing. The chemistry of PLGA (inherently viscosity 0.45-0.60 dl g^{-1}, Mw ~ 38-54 kDa P50/50) comprises the copolymerization of lactic and glycolic acid monomers. Glycolic acid (HOCH2COOH) is the smallest α-hydroxy acid. Lactic acid (HOCH3CHCOOH) is a simple chiral molecule which exists as two enantiomers, L- and D-lactic acid. PLGA solution was prepared by dissolving 100 mg in TFE (2, 2, 2-Trifluoroethanol) (10 mL). The solution was continuously stirred for 30 min at room temperature (25 0C) to get the homogeneous solution and stored at room temperature until further use.

For surface morphology of the thin film, SEM image is shown in figure 2-3 (a), indicating a smooth layer deposition[13]. However, a minor roughness can be seen due to higher ratio of polyglycolide (PGA); which has crystalline structure enabling overall active layer as good sensing candidate. For verifying

chemical structure and purity of material used, FTIR spectra was obtained ranging from 4000 to 750 cm-1, resolution of 4 cm^{-1} and 16 scans per sample. In figure 2-3 (b), EDS data is shown from where elemental data can be seen. Both carbon and oxygen were successfully detected in EDS mapping in addition to Zr which is due to sputtering of sample. The distribution of both intended elements is shown on selected area of sample as shown in bottom images. While for surface nanoscale topography and roughness, direct fabricated sensor was placed in AFM under controlled temperature and humidity of 200 °C and 20%RH respectively AFM 3D images along with average roughness graph were taken, as shown in figure 2-3 (c). The surface morphology was quite flat with average RMS roughness value of less than 3nm.

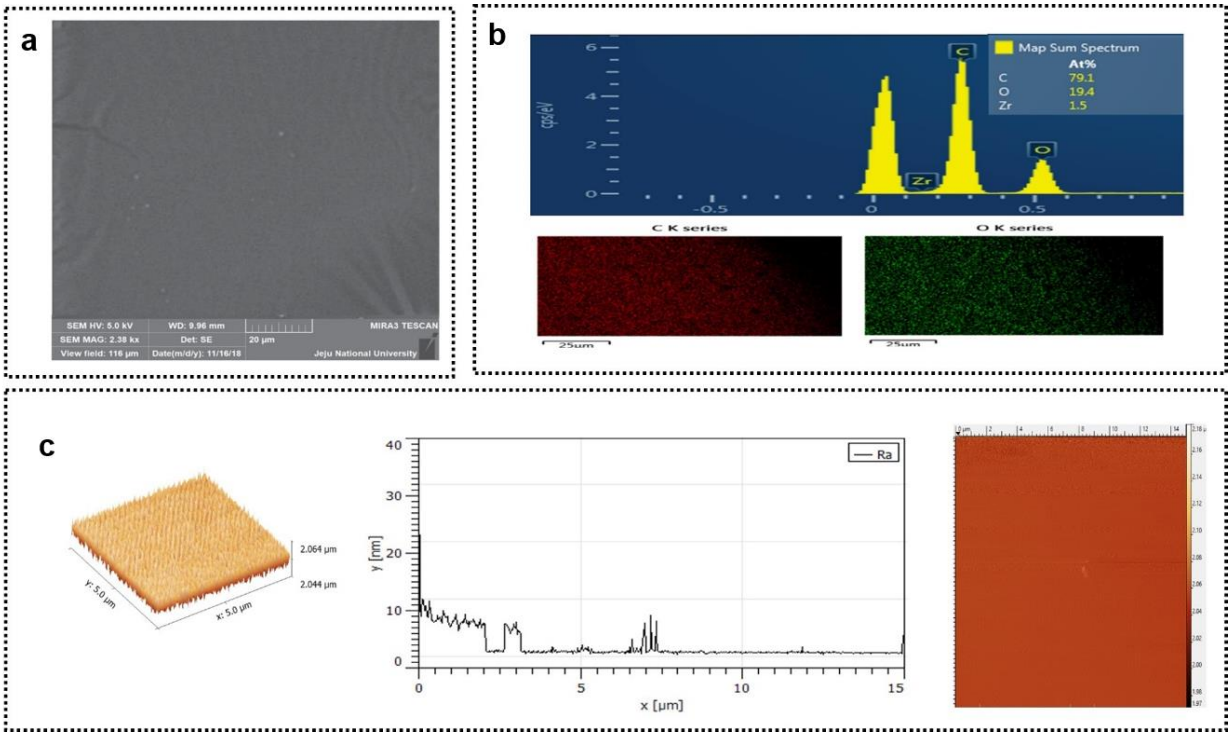

Figure 2-2 Characterization of sensing layer; a) Surface morphology of the samples showing FE-SEM images, b) EDS data, c) AFM 3D profile of film

As shown in figure 2-3 (d), C-H stretch of CH3 and C-H stretch of –C-H- were detected at 2963 cm^{-1}. A band at 1752 cm^{-1} was assigned to stretching vibration of C=O of the strong and narrow ester bond and 1088-1185 cm^{-1} was attributed to C-O stretching which belong to characteristic peaks of the PLGA molecule. Moreover, CH2 e CH2 was associated with 1270 cm^{-1}.

For the design of strain sensors, composites of glycerol and potassium chloride was used. for this, Glycerol was purchased from a pharmaceutical shop in Jeju Island, South Korea. This has similar properties like water and good agent to dissolve the halide salts. The conductive solution was

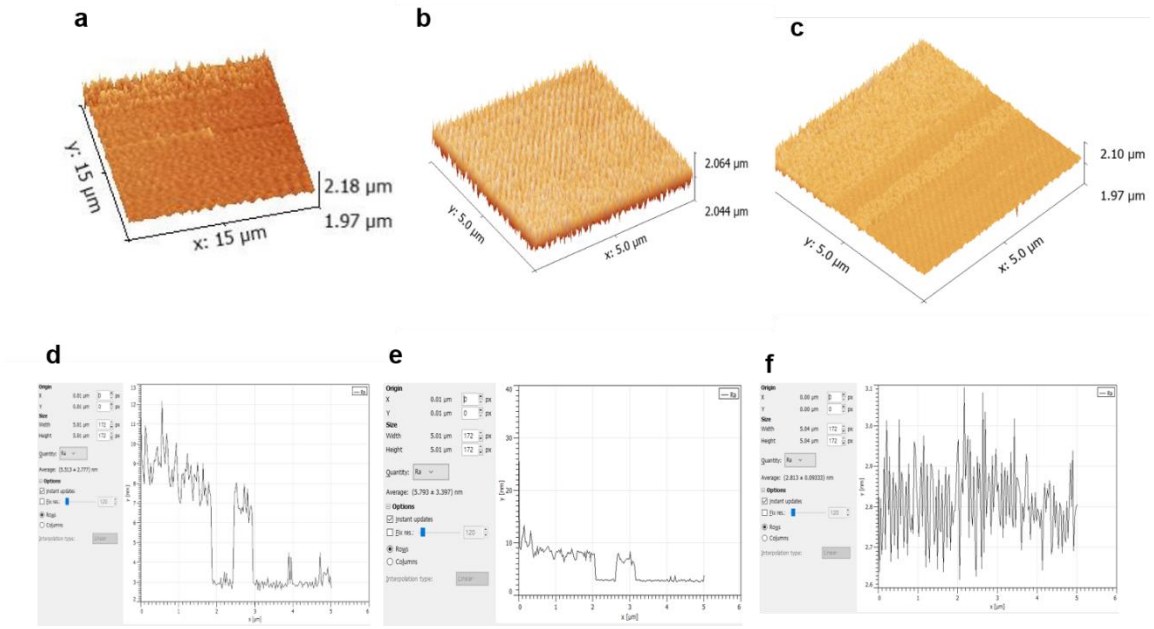

Figure 2-3 a-c) Surface morphology of three different sensor samples, d-f) Surface roughness of three different sensor samples

prepared dissolving potassium chloride (KCl) into glycerol for 4 hrs using magnetic stirrer followed by centrifugal mixing for 10 min. Moreover, the composite has higher ionic conductivity as compared to NaCl and LiCl . Although, the viscosity of glycerol is high even at ambient temperature (~1.4 Pa.s) which normally increases as salt dissolves in it, but KCl has substantially decreased to 0.838 Pa.s when measured using SEKONIC VISCOMATE VM-10A. This augmented the fabricated sensor to better cope with the stretching-relaxing memory effect. The viscosity of pure glycerol and KCL-Gly composite against temperature range of 5.0-50. °C is determined. The composite's viscoelastic property highly depends on the temperature. Moreover for second strain sensor, conductive poly(3,4-ethylenedioxythiophene) polystyrene sulfonate multiwall carbon nanotube (PEDOT:PSS/MWCNT) was used. MWCNT (>98% carbon basis, O.D. 6–13 nm, L 2.5–20 µm) and PEDOT:PSS ink (3.0–4.0 wt.%) were purchased from Sigma Aldrich. Dimethylformamide (DMF) solvent was acquired from Alfa Aesar. For the matrix to hold the conductive liquid through the sinusoidal channel, Ecoflex 00–30 (Young's modulus 70 kPa) purchased from Smooth-on was used. First, different dispersions with MCWNT

concentrations ranging from 0.10 to 0.3 wt% in DMF solvent were prepared. However, on the basis of repeated experiments, 50 mg of MWCNT in 25 ml of DMF was used, which was ultra-sonicated for 0.5 h to ensure that the MWCNT had completely dispersed. To make the composite, PEDOT:PSS (3.0–4.0 wt.%) was poured into the MWCNT solution in a ratio of 2:1, which was ultrasonicated for 2.5 h. Finally, the PEDOT:PSS/MWCNT polymer composite was centrifuged at 1200 rpm for 20 min to separate the large bundles, which significantly affect the homogeneity of the solution. This process was repeated until a clear solution was obtained[14].

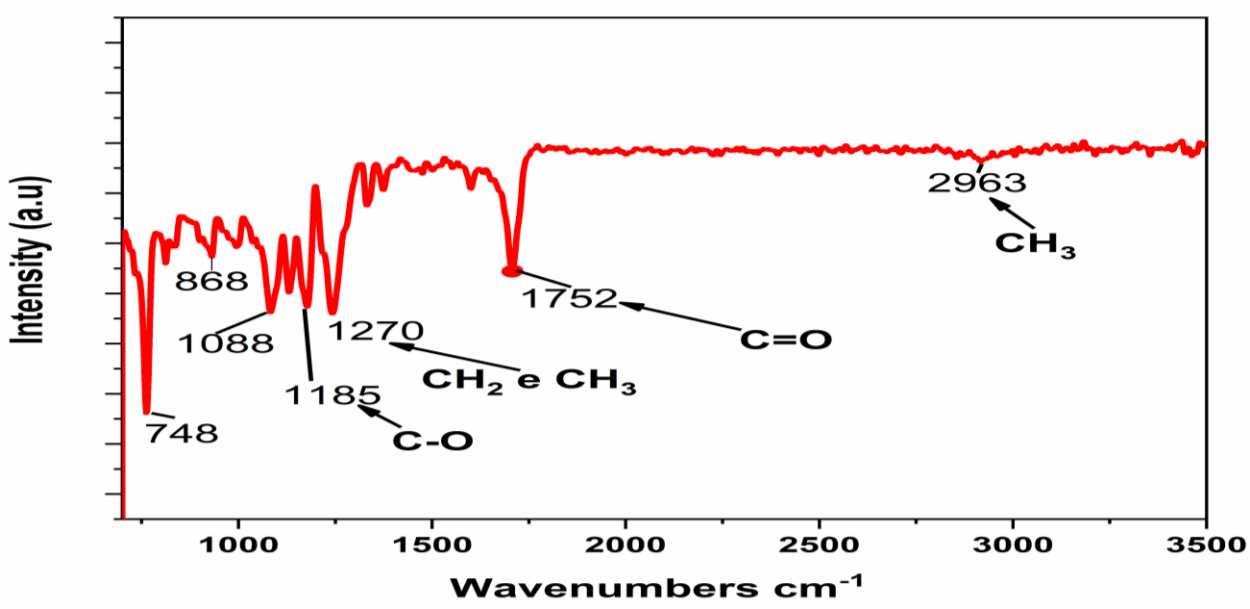

Figure 2-4 FTIR spectrum of pure PLGA showing the chemical composition and purity of the polymer.

2.3.2 Biocompatible Materials

To target the applications like wearable electronics, it is very important that the sensing devices must be biocompatible which must not show any potential hazards to human health[2,17,19–21]. To target wearable applications for humans, it is of considerable importance that the proposed sensor must be biocompatible. This means that the sensor has not only high electrical and mechanical performance but also must not pose any harm to human skin when it is worn[1,22–24]. For this, all the sub-parts of the sensor, including active materials should have possess biocompatibility[25–27]. In this research work, sensing materials are carefully selected which are well-known biocompatible materials. Moreover, to further validate the biocompatibility of the fabricated sensors, biocompatibility tests have been performed. For humidity sensors, biocompatibility of PLGA was assessed by culturing Human small air

way epithelial cells (SAECs) with the as-synthesized films (~100 mm). The film was annealed for overnight on glass petri dish. SAECs viability after 7 days of culture was analyzed and there was no significant difference with a control group (standard cell culture dish). Nuclei were in proper shape stained with DAPI, which indicated that most of the HAECs were healthy. The biocompatibility results of PLGA are shown in **Figure 2-2.**

Moreover, for strain sensor, biocompatibility test was performed using a live-dead assay experiment. For this, human epidermal keratinocytes (HEKp)(Thermo Fisher scientific) human umbilical vein endothelial cells (HUVEC) (ATCC) were cultured on a sensor surface made of PDMS at passage numbers 4 and 5 respectively. HEkp were cultured in serum-free mediaEpiLife® media with 60 µM calcium and human keratinocyte growth supplement (HKGS), and HUVEC were cultured in vascular cell basal medium with growth factors. Sensors containing cells were placed in petri plates with different media and kept at 37 °C in 5% CO2 at 99% humidity for 7 days in incubator. Cell viability was determined by a lived/dead assay kit (Thermofisher). After 48, 96, and 156 h, the sensors containing HEKp and HUVEC were washed with PBS and stained with 2 µl of calcein to stain the incubated live cells for 20 min at room temperature and with 0.5 µl of ethidium homodimer to stain the dead cells for 10 min at room temperature. They were then washed thrice and visualized under a confocal laser scanning microscope. Z-stack images were taken for all the samples[19].

Human primary skin and blood capillary cells were used to test the biocompatibility of the strain sensor. Live/dead assay was performed to check the cell viability over a week. Our results showed good cell viability over a prolonged duration. The sensor did not show cytotoxicity to human skin or blood capillary cells even after 1 week of culture cells on the sensor surface. The survival rates of HEKp and HUVEC were 96.7±1.5% and 97.4±0.9%, respectively, as shown in *Figure 2-2*.

3 Biocompatible Humidity Sensor

This paper reports a fast, linear, all-range sensitive and biocompatible humidity sensor using Poly lactic glycolic acid (PLGA) as a sensing layer for the first time. The device is fabricated using all printing methods. The high definition interdigitated electrode structure was printed on flexible PET substrate by reverse offset printing setup using silver ink, while PLGA ink was deposited using spin coating. IDEs with two different dimensions were printed with three samples of each. There are two major portions in an electronic sensing device, one is the transducer part that comprises of conductive electrodes and the other one is the active sensing portion to detect the target analyte and generate a signal that can be converted to electrical signal through the transducer. The output of sensor is impedance which decreases with increase in relative humidity in a controlled chamber. The results show excellent stability, obvious response to RH for full range from 0– 100%RH with fast response time of 3 s and recovery time of 6 s. Sensor data can be received continuously using smart phone with a Wi-Fi connection with ESP8266 MCUNODE. Sensor's flexibility test was also performed for 5mm mechanical bending radius which showed reasonable consistency with results of flat sensor. The biocompatibility of sensor's active layer was analyzed and confirmed by culturing human small air way epithelial cells for 7 days. To utilize sensor's feature of being biocompatible, it was then used for human respiration monitoring which enabled the proposed device to be strong candidate for wearable electronics and health monitoring applications.

3.1 Sensor Fabrication

Step-by-step fabrication process of the sensor is shown in Figure 3-1. Silver ink was used for electrode fabrication. High resolution interdigital structure was fabricated on PET substrate using reverse offset printing system. Methyl Ethyl Ketone (MEK) was used for removing any dust or fat particles from PET sheets before printing. Two sensors with different thickness and spacing are developed with names sensor-1 and sensor-2. Sensor-1 has total of 40 fingers (thickness of 50um, spacing of 40um and length of 8mm) while sensor-2 has 10 fingers (thickness of 250um, spacing of 240um and length of 8mm). Three samples of each sensor type are spin coated with PLGA ink with fixed RPM set at 1000, 2000

and 3000 respectively. Optimized results were achieved with 2000 RPM with sensor-1. All sensor samples were placed in a furnace with preset temperature of 100 °C for 12 hours for films to be properly cured.

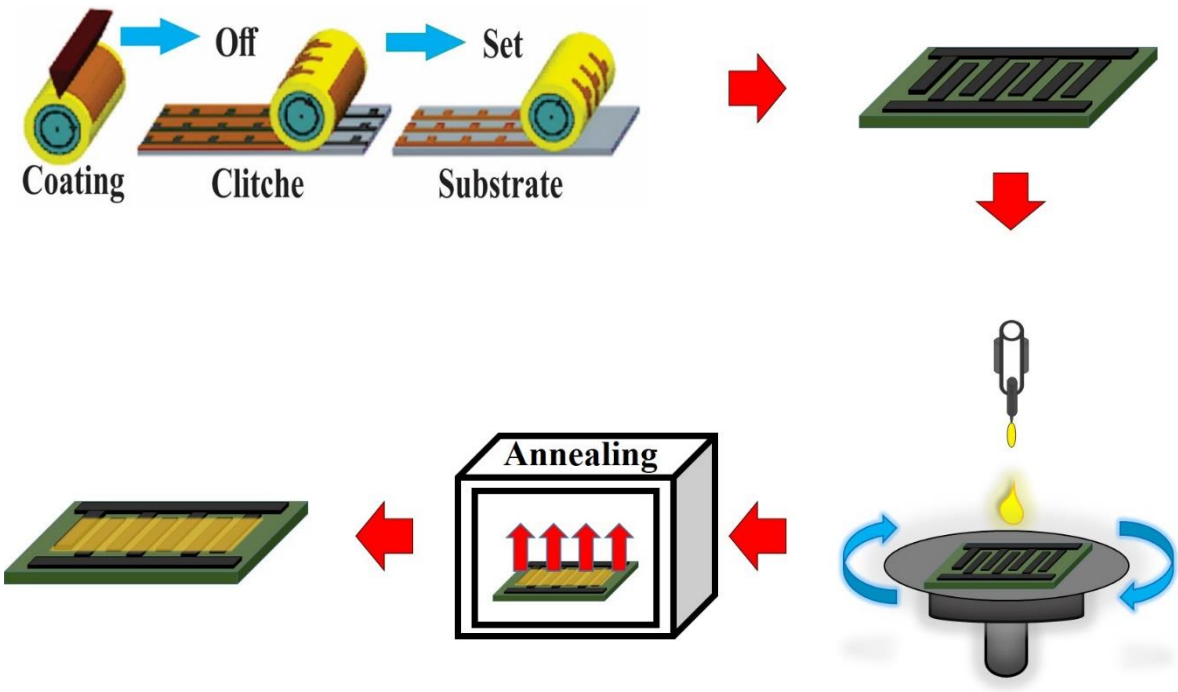

Figure 3-1 Step by step fabrication process of humidity sensor; reverse offset printing of silver IDEs (top right), fabricated IDEs (top right) are then deposited with PLGA ink using spin coater (bottom right) followed by film annealing (bottom center) and fabricated device (bottom left).

3.2 Electrode Fabrication

Electrode fabrication requires the printing system to print patterns in any shape and of any size with high accuracy and repeatability[27–31]. The electrodes need to have high electrical conductivity and smooth finishing. Three major printing techniques were used to print the transducer electrodes for our sensing devices. Highly accurate and conductive electrodes were fabricated through reverse offset printing. Silver conductive ink was used by Silverjet DGH ink for reverse offset (viscosity: 1.5cps, surface tension: 24.4mN/m, dispersion matrix: octane based). Reverse offset printing works on the principle of transferring a fixed design pattern from the host substrate to the target substrate through a PDMS blanket roll. Multiple design of interdigitated transducer (IDT) electrodes were prepared and

the cliché was fabricated for each design [10]. The process details and working principle of the printing system are explained in ***Figure 3-2***. The fabricated electrodes by reverse offset printing were cured at 200 °C for 2 hours for all devices.

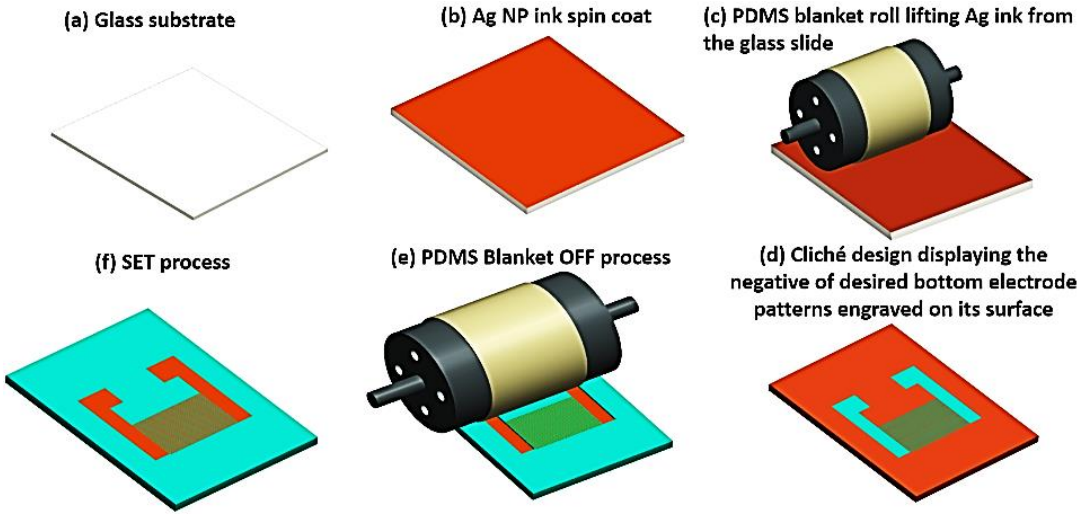

Figure 3-2: Step by step fabrication process of reverse offset printing for electrode fabrication.

The advantages of using reverse offset printing method is that this system is mass production compatible[32] and if the process parameters are optimized carefully[33], it is capable of printing very high quality patterns that can compete with the conventional lithographic techniques. Pattern sizes of up to 20 µm were printed successfully with very high quality finish[34–39]. The system was mostly used to print the bottom transducers for the sensing devices and then the top sensing layer was deposited onto them through other printing methods.

3.3 Characterization setup

Custom-built controlled environment box. Setup has capability to control its humidity form 0% RH to 100% RH using Proportional Feedback Controller (PID). Dry nitrogen gas was used to decrease the humidity to minimum value of zero or change to any other value of choice whereas for achieving humidity level up to 10% RH, compressed dry air was preferred. Desktop humidifier was used to add water vapors to the chamber for increasing the RH. All inlets were electronically controlled using Electronic mass flow controllers (MFC) except dry nitrogen gas which was manually regulated. The response of sensor was continuously logged to desktop computer using USB connection and smart phone using local WIFI network. There was an average change of 2%

RH and around 50 data points from maximum %RH to minimum and vice versa. A commercial sensor DTU-21D is used as reference and feedback for PID controller. For measuring sensor's impedance, handheld LCR meter (LCR-916, GW INSTEK) was used to display real time graph in addition to data logging to computer. The meter was set to get sample after every second and could generate 0.6 Vrms AC output with five different frequencies (100Hz, 120Hz, 1 kHz, 10 kHz, 100 kHz). Data from reference sensor was received using ESP8266 (WIFI enabled microcontroller board) that continuously sent data to computer using USB communication and LCR meter logged data using its own commercially available software. Temperature of chamber is maintained at 25 0C during the whole experiment. To achieve remote monitoring, android application has been designed using MIT app inventor online platform that receives real-time values of impedance and displays on phone's screen against time. The details of setup are shown in *Figure 3-3*.

3.4 Working Mechanism

The working principle of proposed RH sensor is based on impedance change when water molecules are trapped by the sensing layer. Sensor's behavior is to decrease impedance against increasing relative humidity of controlled chamber[40–44]. The resultant effect of capacitance of fabricated film and resistance of electrodes provides the impedance magnitude. So, increase in RH value either gives rise to dielectric constant or increase in conductivity (decreasing resistance). The mechanism is shown in figure 5. Humidity sensing can be divided in to two parts; initially sensor's dominant behavior is due to chemisorption which causes the generation positive ions (H^+). Every water molecule trapped by sensing film leads to the formation of lactic acid-glycolic acid oligomers resulting in acid carboxylic end group [45], causing increase in ionic conductivity which enables protonic conduction current to flow between electrodes. This also makes the sensing very fast. Secondly the decrease in impedance is also due to physisorption which is normal phenomenon reported in many of the RH sensing devices [31,32,44,46].

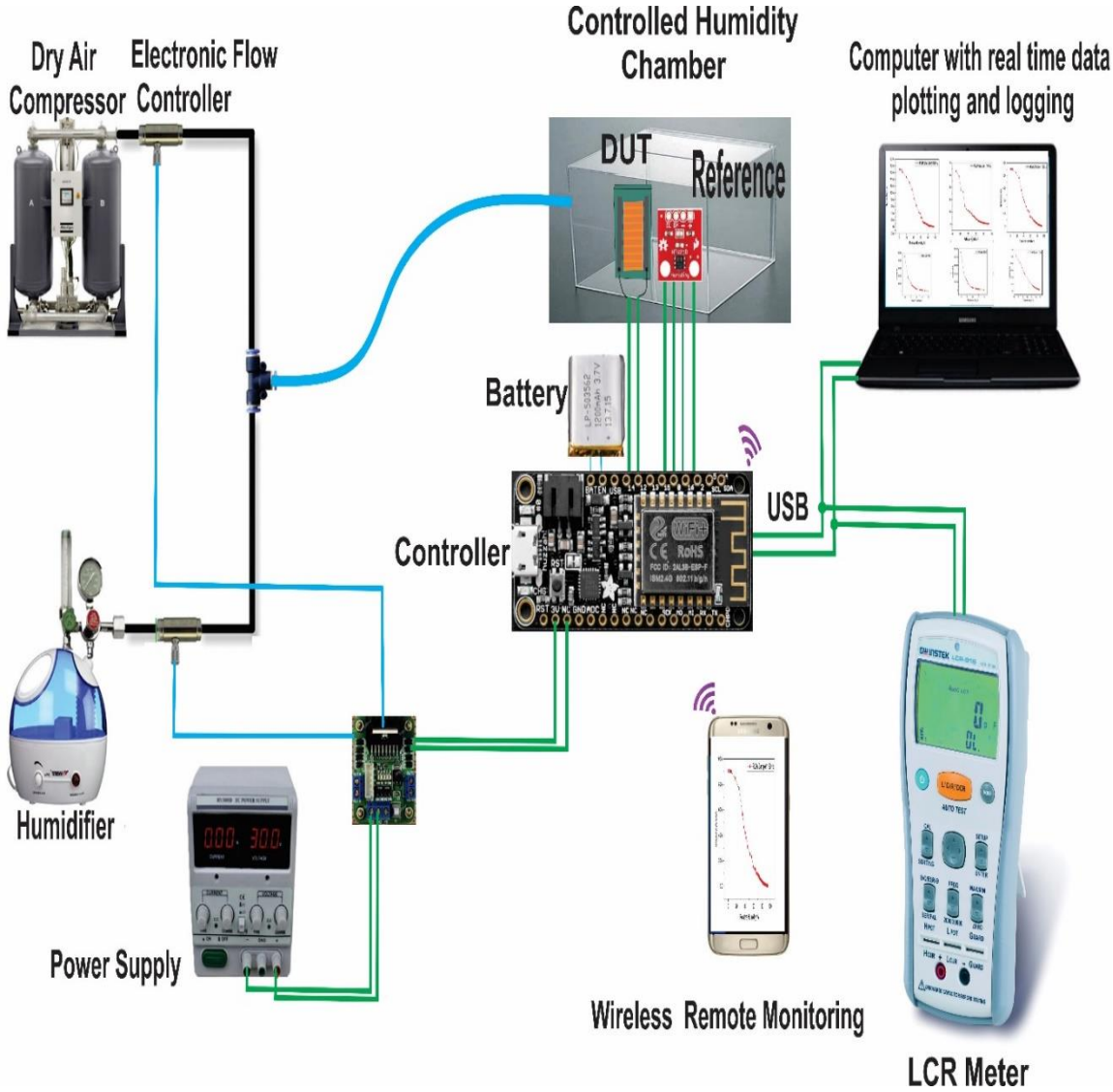

Figure 3-3 Custom developed characterization setup schematic used for the measurement of sensors response against change in relative humidity.

3.5 Sensor's Electrical Response

Sensor's electrical performance is analyzed by measuring the output impedance against change in relative humidity of electronically controlled chamber. Obtained results suggest the behavior of decreasing impedance as the level of water vapors increase. Different thicknesses fabricated sensing layers exhibited different intrinsic impedance while showing dominant behavior of inverse relation between thickness and impedance. The impedance response against relative humidity change of sensor-1 and sensor-2 at two frequencies (1 kHz and 10 kHz) are shown in *Figure 3-5*.

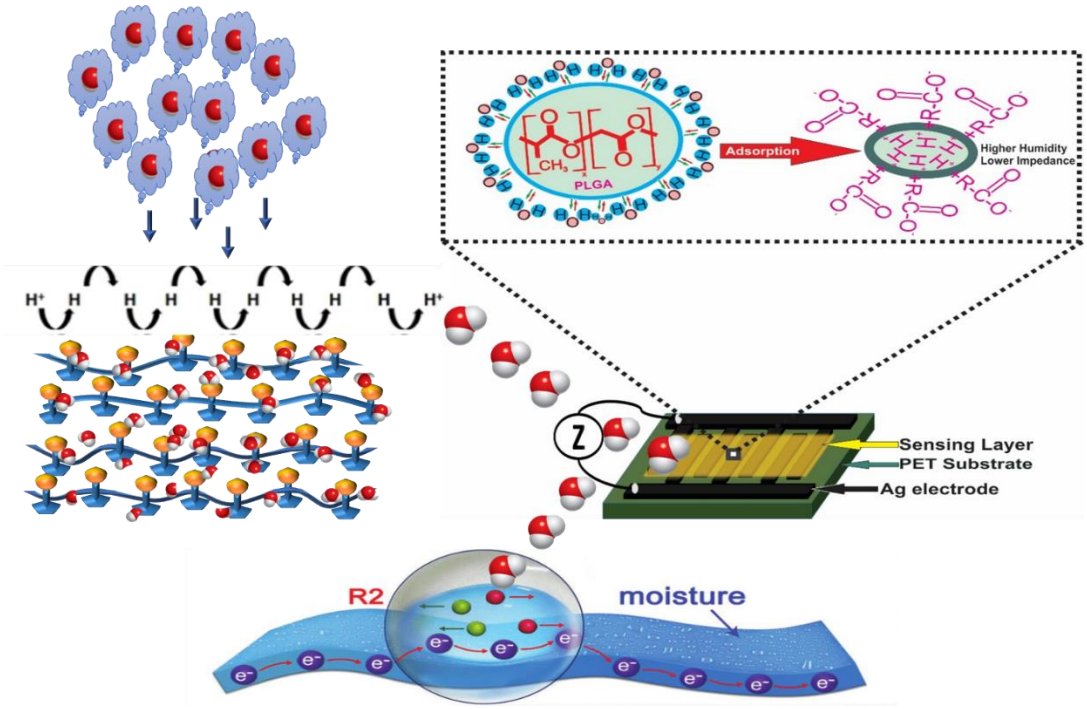

Figure 3-4 Humidity Sensing Mechanism

The results show that there is inverse relationship between impedance of sensor and relative humidity of the chamber in which sensor is placed for testing. Both sensors' response is highly sensitive and linear throughout the humidity ranges. The overall response of each sensor can be divided into two unequal parts; the first part of each sensor is highly sensitive and undergoes rapid change of impedance, however in second part due to enough saturation due to adsorption, the change in impedance is decreased. To verify the consistency of fabricated sensors, three samples of each sensor type were analyzed. Results shown in Figure 3-5(e-f) pose great level of coherence which is highly required for the commercialization of any device.

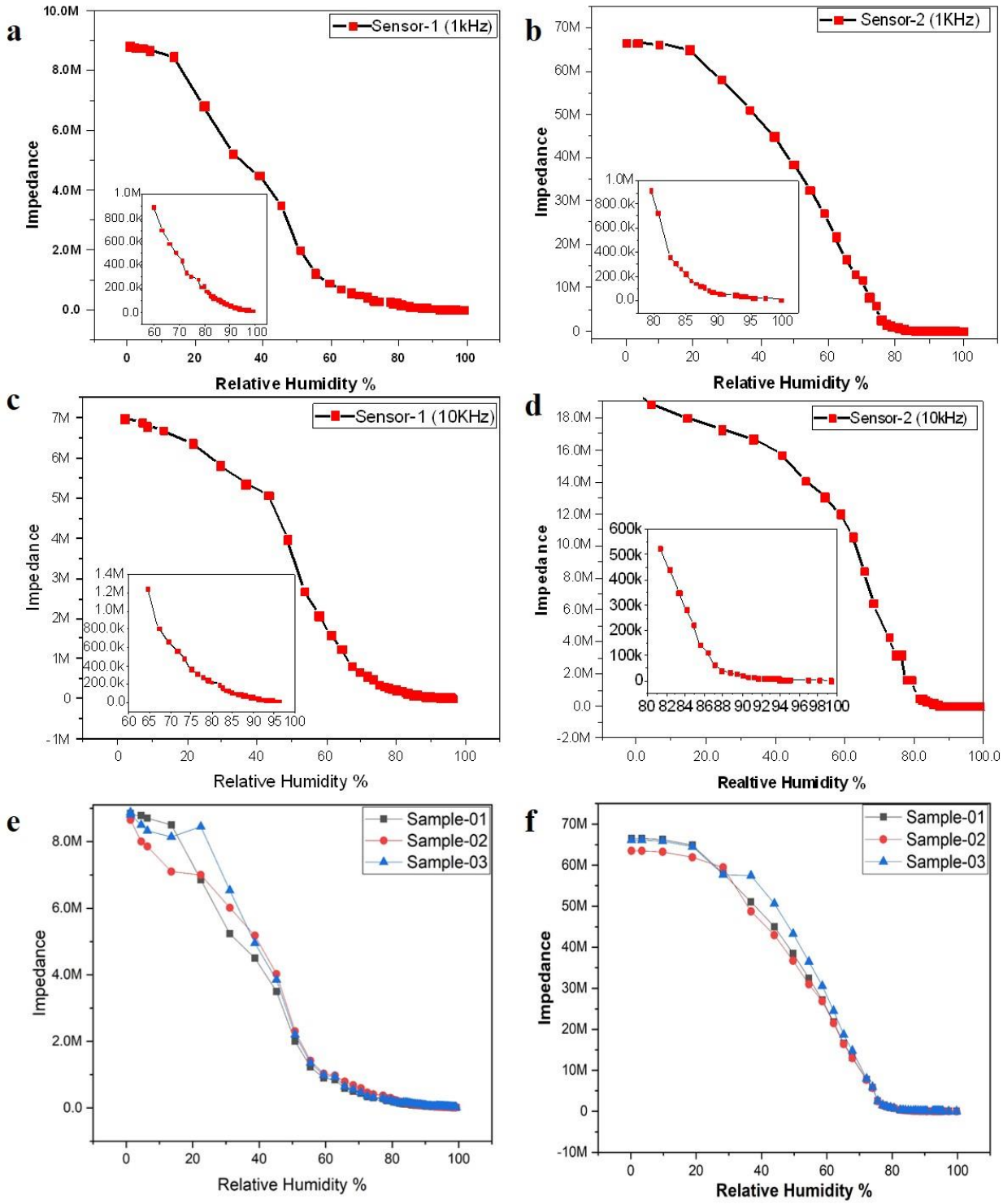

Figure 3-5 Impedance response of Sensor-1 and sensor 2: a) Sensor-1 at 100 Hz b) Sensor-1 at 1 kHz c) Sensor-1 at 10 k Hz d) Sensor-2 at 1 kHz e) Sensor-2 at 10 kHz

3.5.1 Sensor's reproducibility

Repeated cycles of the rapid humidification and dehumidification were performed to determine the transient response of sensor and response/recovery time. Cyclic behavior, the sensor's surface was placed near dry nitrogen gas valve and humidifier tube. For increasing the humidity the tube was placed at a distance of ~20mm form the perpendicular vector area of sensor. The process was done

quickly by opening and closing valves of humidifier and gas cylinder. The results for cyclic performance and transient response are shown in *Figure 3-6*. The response and recovery times of sensor were determined using transient response shown in *Figure 3-6*(b-c). The output of the sensor was directly logged against real time change. Commercial humidity sensor's reading was continuously checked to properly achieve RH values of ~10% and 90%; response time is the time taken by sensor to reach from 10% to 90% whereas vice versa for recovery time. Repeated sensor's pattern about 140 seconds gave a highly stable transient response with response time of 3 s and recovery time of 6 s. Both values are highly suitable for various applications specially that requiring high response time like in the case of personnel health monitoring.

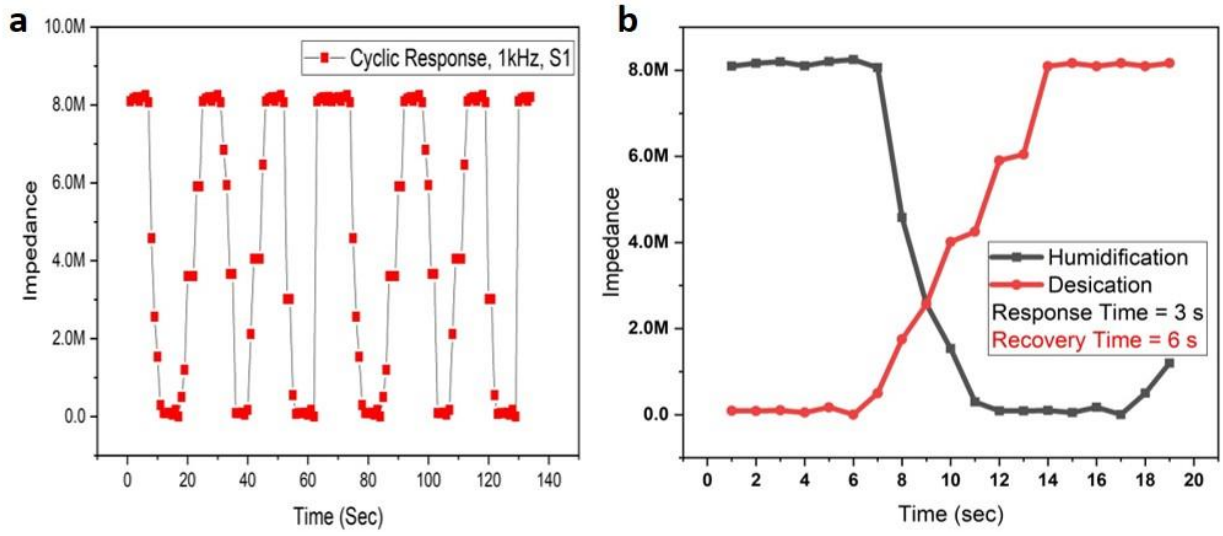

Figure 3-6 Impedance response curves for the sensor showing (a) multiple cycles of humidification and desiccation and (b) Transient response for response and recovery time calculations

3.5.2 Sensor biocompatibility Test

The biocompatibility of any sensor plays a decisive role, whether a sensor should be used a human wearable device or not. For the proof of concept, biocompatibility of PLGA was assessed by culturing Human small air way epithelial cells (SAECs) with the as-synthesized films (~100 mm)[47]. The film was annealed for overnight on glass petri dish. SAECs viability after 7 days of culture was analyzed and there was no significant difference with a control group (standard cell culture dish). Nuclei were in proper shape stained with DAPI, which indicated that most of the HAECs were healthy. The SAEC's were stained with Goat anti-Mouse IgG (H+L) Highly Cross-Adsorbed Secondary Antibody, Alexa Fluor

Plus 488 to check the cell morphology and nuclei were counter stained with and 4′,6-diamidino-2-phenylindole (DAPI), Followed by fixing cells immunohistochemically using 4% Paraformaldyhye for 15 minutes and rinsed three times with DPBS. After washing samples were blocked with 0.1% bovine serum albumin (BSA) solution for 1 hour at 37°C and were incubated with for 90min at room temperature.

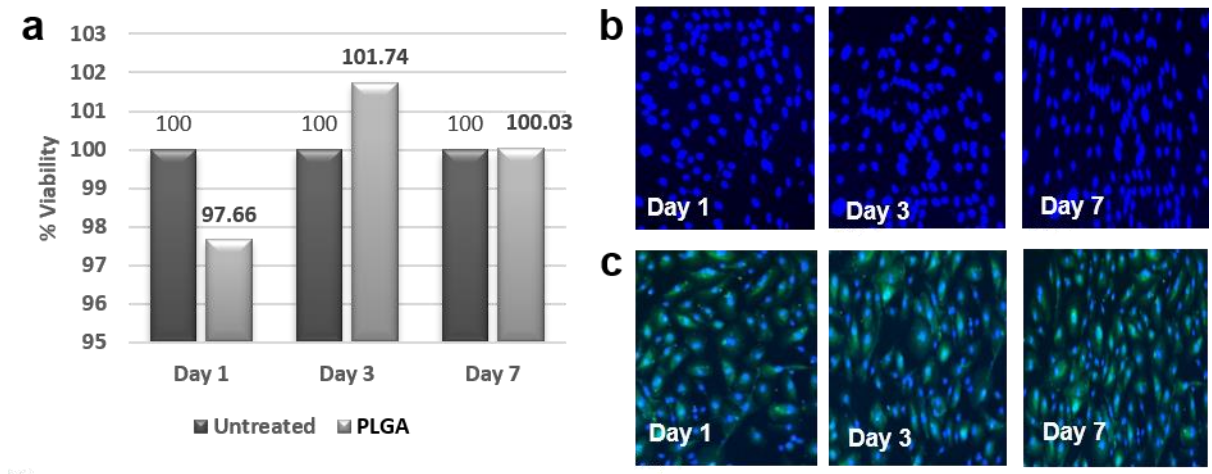

Figure 3-7 Biocompatibility of PLGA. A) % Cell viability of SAEC's cultured on PLGA films for 1,3 and 5 days, B) DAPI stained nuclei exhibiting proper morphology, C) Fluorescence images of stained SAEC's cultured on PLGA films.

3.5.3 Human Breathing Monitoring

To implement the practical application of designed fabricated sensor, respiration monitoring is achieved due to the fact that sensor is eco-friendly and biocompatible[48,49]. The lung epithelial cells were used to verify the biocompatibility of PLGA which augmented its use for breathing analysis of human being. To assess the respiration performance, the sensor was placed under the volunteer's nose. Response was divided in to four categories; normal breathing, deep breathing, fast breathing and intentional delay between two respective breathing style known as apnea so that the RH value is stabilized. The respiratory response is shown in *Figure 3-8*. Sensor exhibited quick impedance variation with frequencies of 0.18 Hz, 0.21 Hz and 0.63 Hz for normal, deep and fast breathing respectively. Sensor achieved highest impedance variation in deep breathing as in such case; more water molecules are exhaled out and are trapped by sensor surface. During this experiment, we have ignored the effect

of temperature as there will be very less effect of normal body temperature on sensor's output impedance, so in that case the sensor can be attributed to be only sensitive to water vapors[50–53].

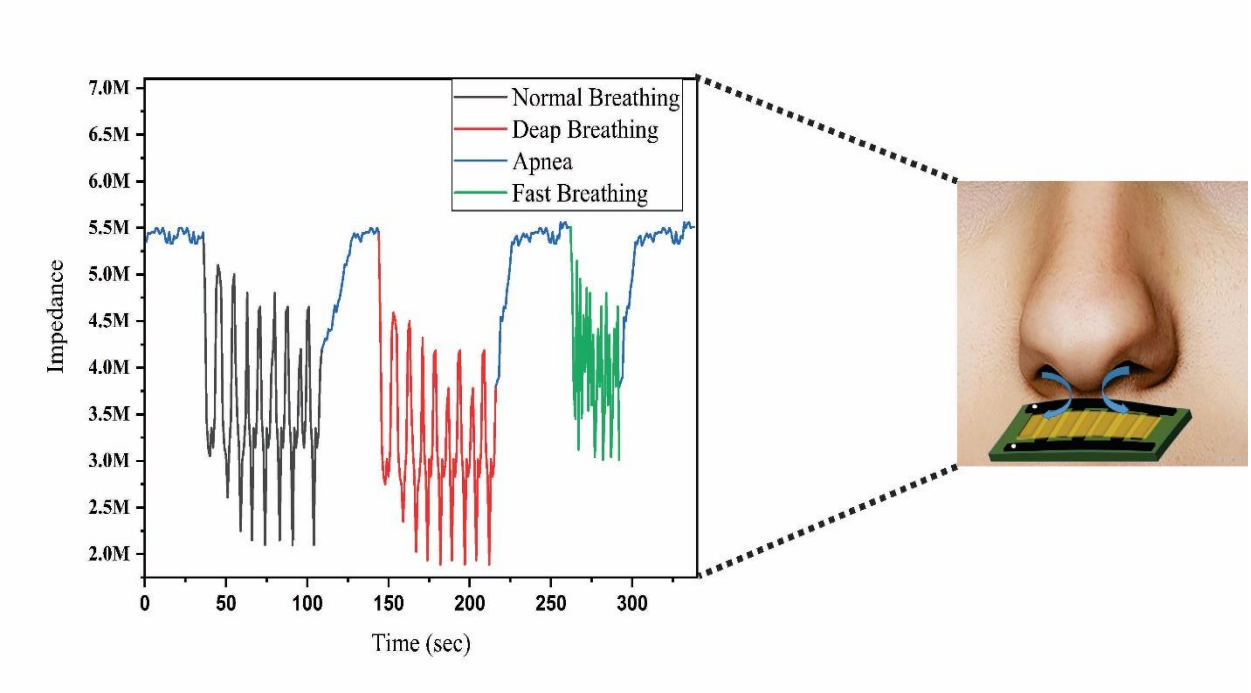

Figure 3-8 Breathing characteristics by impedance response to normal, deep and fast breathing; Time-dependent impedance variations against breathing of a human sample.

3.5.4 Sensor's Flexibility Test

In *Figure 3-9*, the flexibility of sensor is analyzed. Due to high flexibility of PET substrate which enabled the overall device flexibility[54–57]. For the proof of concept, bending radium of 5mm was demonstrated. The performance of sensor was consistent, stable, linear and sensitive for the wide range which supports the integration of sensor for various application especially wearable devices targeting health monitoring. Overall, the proposed sensor performed more effectively than reported biocompatible sensors with optimum figure of merit by achieving fast response and recovery time, sensitive to whole humidity range, flexibility and biocompatibility. The sensor utilizes a novel material which is mostly used in drug delivery and other biological applications and can prove to be a good choice for different applications, more specifically for health monitoring where biocompatibility and other performance factors are highly required[10,46,58,59].

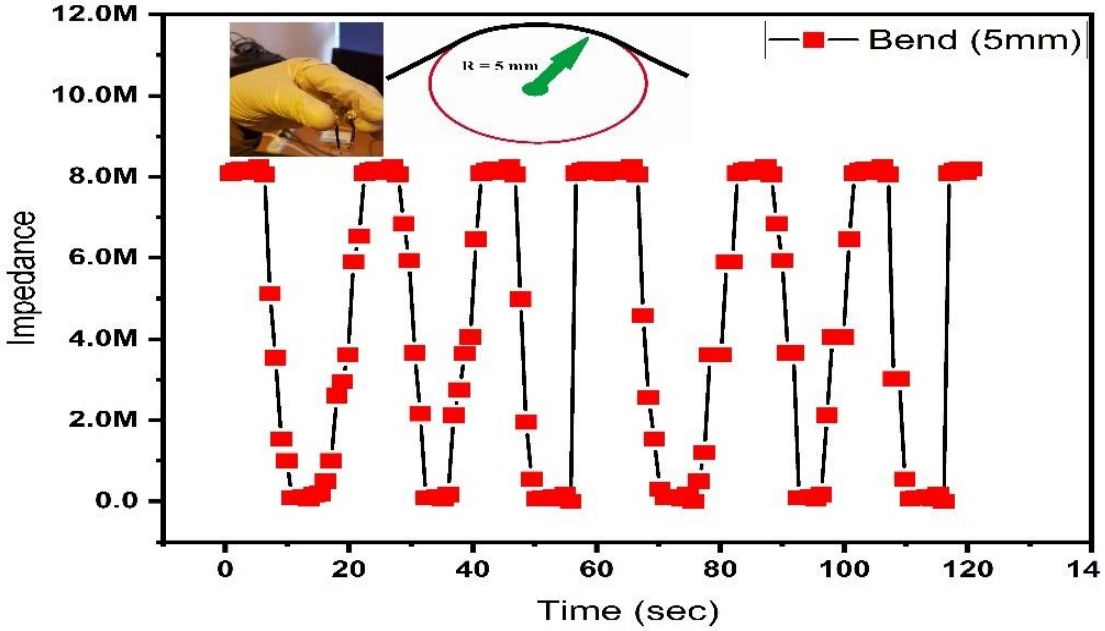

Figure 3-9 Bending test of sensor for multiple cycles, inset images (left: optical image of bending sensor, right: illustration of bending of 5 mm).

4 Body Posture Detection Sensors

Strain sensors have gained significant importance in fields such as human health monitoring, hand and limb movement detection, blood pulse monitoring, respiration rate monitoring, feedback-enabled soft robots, flexible touch screens, and electronic skin[45,60–68]. Conventional strain sensors utilize a mature technology by exploiting various buckling, meshing, and interlocking films and foams in graphene and carbon[47,69–71].In addition, inorganic conductive materials have also been explored, which contain silver, gold, and ZnO nanowires[72–78]. In such sensors, the fundamental working mechanism is based on the transformation of conductive networks along with the elongation of an elastic material[79–81]. These sensors have high sensitivity changes in strain; however, this not only makes the fabrication process complex but also results in large hysteresis, which makes the measurement process less precise[82–86]. To resolve this problem, percolation networks of inorganic materials have been used to develop piezocapactitance-based strain sensors. These sensors have improved linearity and less hysteresis but lack sensitivity with a gauge factor (in the range of 1.0 or less)[14,87–90].

Recently, soft strain sensors have been developed using conductive liquids. These sensors have the advantages of a compliant nature, low cost and high suitability of mass production, which allow them to efficiently operate in soft electronics applications. Conventional fluidic-based sensors are fabricated using three types of conductive liquids, electrolytes based on salts, such as KCl-glycerol, ionic liquids, and liquid metals[91–95]. Moreover, the working principle of such sensors is based on changing electrical resistance due to the changing length of the liquid path caused by stretching, bending, and other forms of deformation[96–100]. Conductive carbon greases have also been reported in the literature; however, in such a scenario, shear has a significant effect on the resistivity of conductive solutions; thus, they have a large memory effect owing to their viscoelasticity attributes. Moreover, researchers have explored eutectic gallium-indium alloy (EGaIn) and GaInSn liquid metals to fabricate strain sensors. In fact, these liquids have a low melting point and good electrical conductivity of 3.4–3.5 × (106 S m^{-1}), and have been used in different robotic and human motion monitoring applications[101,102]. However, the main hurdle to their mass production is their high cost. Hence, work is still needed to realize a

fluidic strain sensor that can achieve a robust blend of features such as less hysteresis, simple design structure, fast response and recovery time, large strain sensing range, and most importantly, biocompatibility, which is an indispensable requirement for the risk-free usage of sensors for health monitoring[103–105].

4.1 Soft Strain Sensor based on KCl-glycerol

In this research study, we explore sensing capability of a novel biocompatible ionic liquid composed of potassium chloride and glycerol. The proposed conductive liquid minimizes the hysteresis problem to 4.23%, as compared to existing biocompatible solutions, due to substantially less viscosity of composite. Herein glycerol, a common material used in cosmetics, is a good solvent for halide compounds that breaks KCl into potassium cations (K^+) and chlorine ions (Cl^-) which causes the resultant composite to be conductive. The proposed design structure is based on five-half-cycle sinusoidal channel pattern which further achieves high sensitivity in addition to high linearity, stable measurements and less memory effect. The sensor has been tested under full range relative humidity (0-100% RH using our custom-made electronically controlled chamber. As proof of concept the device was successfully used in the 3D printed single joint-robotic leg using PLA filament as a feedback sensor inside water. The device showed coherent response in respect to angular movement of 30 degree. This confirms the underwater application of our proposed sensor for high end under-water robotic feedbacks. Moreover the sensor was also used for wearable electronics more specifically monitoring the water drinking activity of a human. The device was characterized in the temperature range of 10.0 – 40.0 ˚C.

4.1.1 Sensor Fabrication

The sensor fabrication mainly contains two steps. Firstly, the design of a highly stretchable material, which herein, ecoflex 00-30 (Young's modulus 70 kPa) and high failure strain of 900%, Smooth-on) has been. The silicon elastomer is commercially available in two parts, which when mixed in weight ratio of 1:1; the highly flexible rubber comes into shape. Secondly, the fabrication of sinusoidal pattern, fused deposition modeling (FDM) based 3D printing was used to create the mold as shown in figure 1a. Total of five half-cycles were printed in the mold using Creality CR20 printer and ABS filament.

Before pouring of elastomer into mold, it was mixed for an hour, followed by stirring, degassing. The filled mold was cured on room temperature in 4 hours after which it was peeled off in a careful manner. The two silicon-coated wires were already attached with the mold as our target was to make our fabricated device waterproof

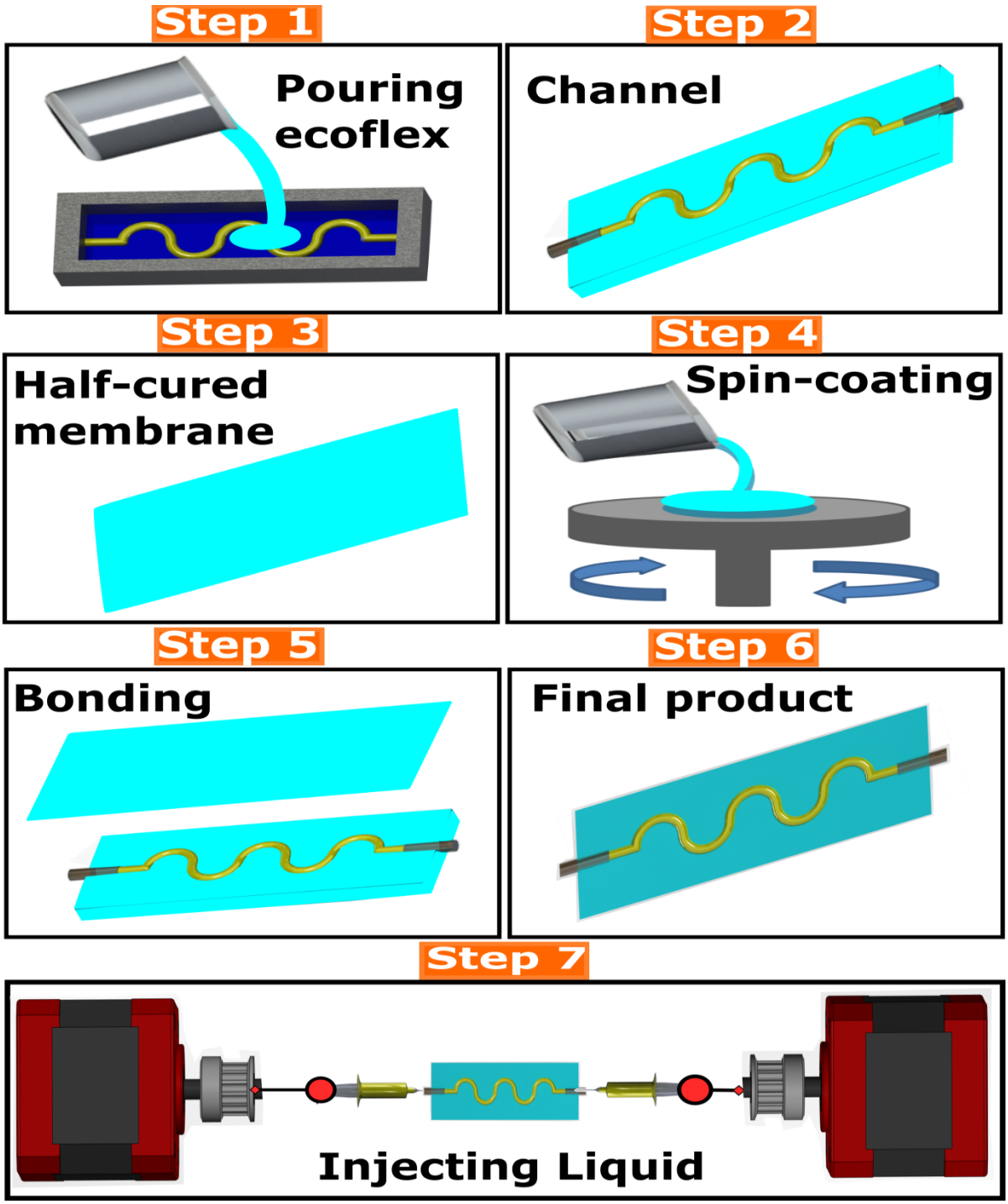

Figure 4-1 Step by step fabrication process for strain sensor. a) 3D printed mold with silicon coated wires attached is filled with ecoflex 00-30 (1), cured elastomer with patterned channel peel off (2), spin coating exoflex for thin membrane fabrication (3), half-curd thin membrane (4), combining sensor substrate and half-cured membrane for bonding in natural environment (5), fabricated sensor final

desired shape and form (6) Injecting conductive liquid inside the fabricated channel using custom-made stepper motor controlled 2 syringes.

so it was highly required to avoid separate wire connections. In second step, a thin film was spin-coated on a flat substrate using the same elastomer, which was then half-cured and wet-bonded with the first part in ambient temperature with some nominal pressure so there is no leakage for air or liquid to inter-cross. Finally two syringes were used to fill the channel with ionic-liquid. It required huge synchronization between the movements of both syringes as otherwise bubbles were trapped in the liquid-channel which severely degraded the performance of sensor[106–109]. To resolve this issue, we connected the two syringes with stepper motor driven stages which were programmed using C++ on Arduino Mega board as shown in figure 1b. This helped ensuring there was no bubble. Finally the tiny holes created due to infilling of liquid, were closed using epoxy glue. Step by step fabrication process is shown in Figure 4-1. The area of sensor was 54mm x 20mm and the patterned sinusoidal channel has diameter of 2mm with peak to peak height of 12mm and half-cycle width of 10mm. The sensor has total of five half-cycles. Various optical images of prepared devices (with infilled sensing liquid composite) in different deformation styles have been shown Figure 4-3 e-g. The device showed high level of flexibility and capability of undergoing high tensile strain.

4.1.2 Working mechanism

The working principle of Gly-KCl is shown in Figure 4-3 which shares concept from a well-known phenomenon normally taking place in water; the decomposition of salt in to positive and negative ions [11093]**.** As glycerol shares major properties with water, it also breaks KCL into potassium cations (K^+) and chlorine ions (Cl^-). The free ions in glycerol develop the conductivity in liquid. Once the device is deformed by applying axial strain, the device length increases and simultaneously the cross-sectional area is decreased, as a result the resistance is increased. The same affects the viscous liquid in channel whose resistance changes based on the intensity of deformation. Applied tensile strain widens the space among the free ions in aqueous solution which impacts the overall resistance of liquid from end-to-end that is measured using a handheld meter.

4.1.3 Device Structure optimization

In order to optimize and check different effects inside fabricated strain sensing device, finite element analysis (FEA) was carried out in COMSOL 5.4. First the channel which was filled by solution of Gly-KCl was designed and meshed in the COMSOL by utilizing laminar flow and electrostatics modules. The purpose of this analysis was to check the velocity and pressure inside the channel by applying voltage. Once the fluid entered the channel, it became stagnant; the voltage 0.6V was applied to one end while other end was grounded for taking strain sensor measurements[84,111–114].

As a summary of this chapter, we have developed a highly flexible, linear, stable soft strain sensor based on the composite of glycerol and potassium chloride using simple and cost-effective fabrication technique. Five-half cycle sinusoidal channel was fabricated using highly elastic ecoflex 00-30 with help of mold 3D printed using commercial printer. The sensing liquid composite was quite stable with lower viscosity that helped our sensor to be less prone to hysteresis effect as low as 4.23%. Sensor's electrical and mechanical characterization was carried. The developed device attained a linear and reproducible response up to 100% strain with maximum GF of 2.7 at full stretching. The device showed excellent performance even after the 8000 cycles stretching and relaxing up to 25% of axial strain using our custom made tensile testing machine. The fabricated device was sensitive to all strain values with the range of 0- 100% with high relative resistance change up to 2.75. The response of device was analyzed up to 5 Hz of speed which was consistent which make the proposed design suitable for human motion detection applications; moreover the device was characterized in different environment varying humidity and temperature, the device stayed highly stable in %100 RH and in temperature range from 10-40 ^{0}C. The optimization of design was performed in COMSOL 5.4 to analyze various effects like pressure distribution, velocity distribution of liquid strain and stress using FEA. Lastly, the device was used in three diversified applications; as high end robotic feedback strain sensor, water drinking activity monitoring and human finger bending sensor. The results positively support the proposed sensor to be strong candidate for applications like wearable electronics and feedback sensing for robotics.

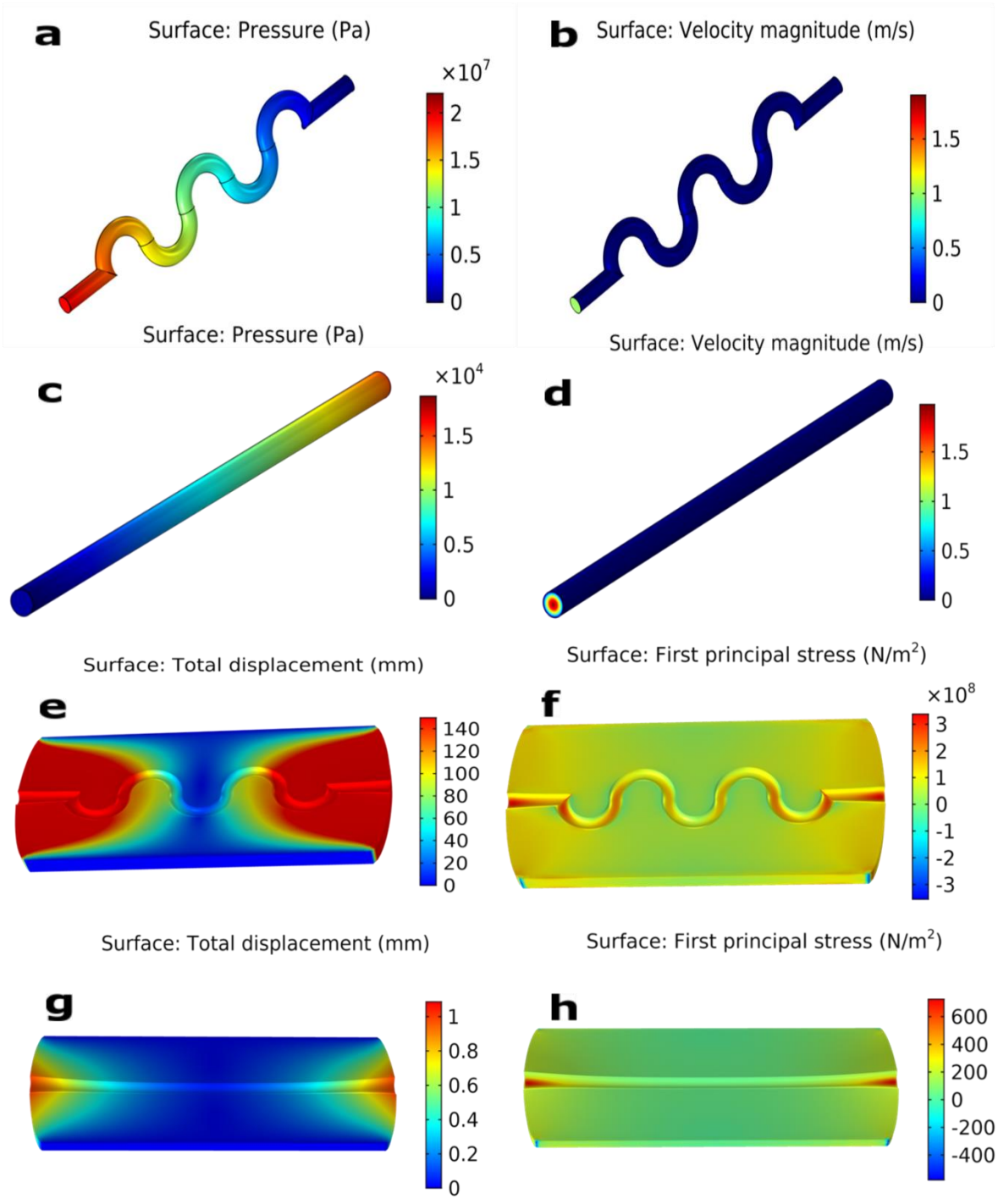

Figure 4-2 FEA carried out in COMSOL 5.4 of proposed device and simple straight channel results (a) Pressure (pa) distribution of proposed design (b) Velocity distribution of proposed design (c) Pressure (pa) distribution of straight channel (d) Velocity distribution of straight channel e) displacement effect on proposed design f) stress effect on proposed design g) displacement effect on straight channel design h) stress effect on straight channel design

The electrical response of strain sensing devices was analyzed by measuring the resistance between device's two end terminals against axial stretching and relaxation strain. The device was the measured

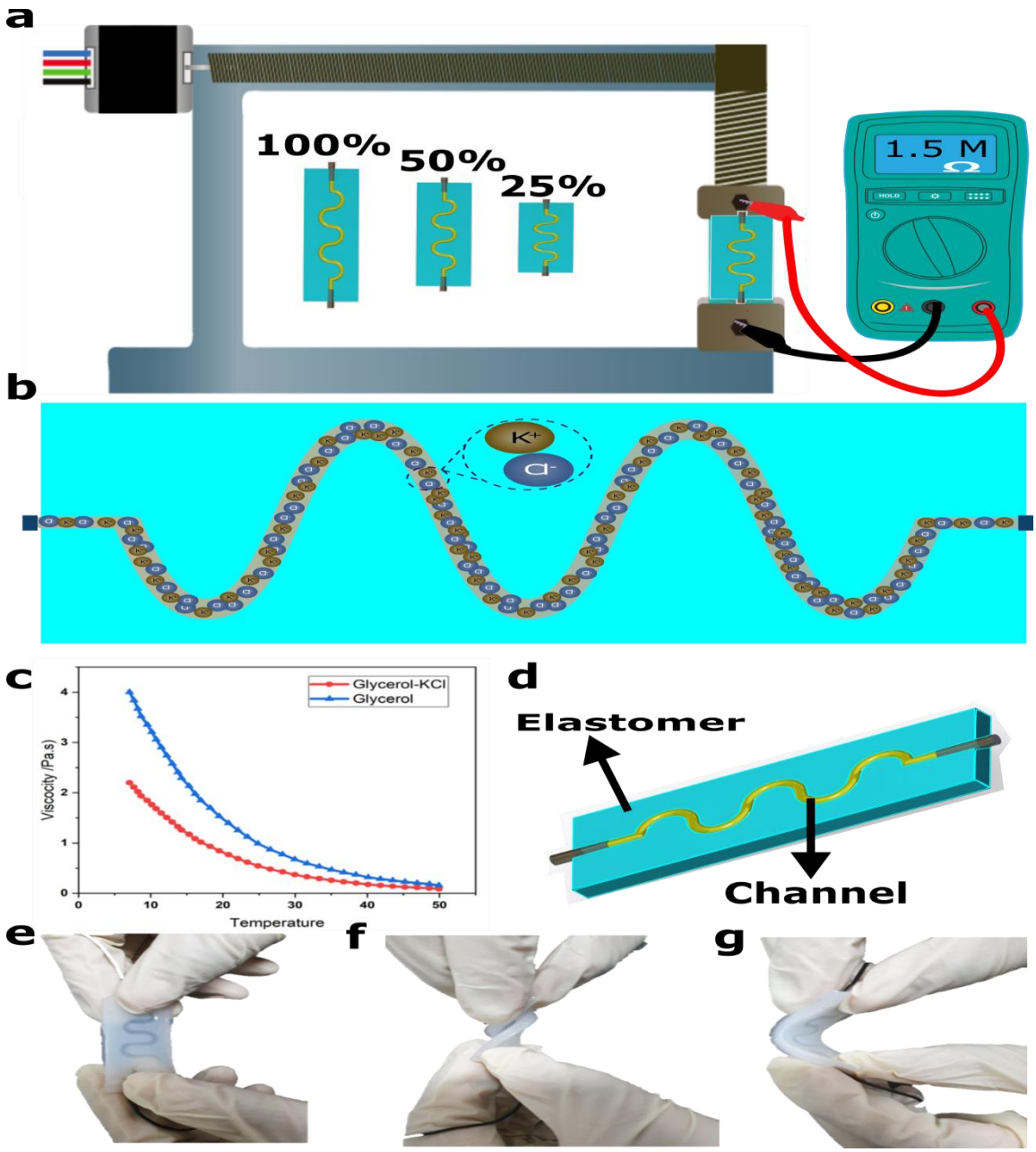

Figure 4-3 a) custom made Tensile Strain Characterization setup with capability of applying variable strain with programmed frequency, b) Working Mechanism of fabricated sinusoidal channel patterned strain sensor c) Viscosity of pure glycerol and composite glycerol-KCl against temperature range (10-50 ^{0}C), e-g optical images of fabricated sensors in different mechanical states

resistance values were then converted to relative change of resistance $\Delta R/R_0$ which was plotted against applied strain. The device was tested up to stretching of 100% strain which showed high sensitivity with almost three times resistance change with full strain of 100%. The response was highly

linear during loading and unloading cycles. The hysteresis incurred in sensor's response was calculated using formula mentioned in equation (1) [115].

$$DH = \frac{A_{Loading} - A_{Unloading}}{A_{Loading}} x100 \quad (1)$$

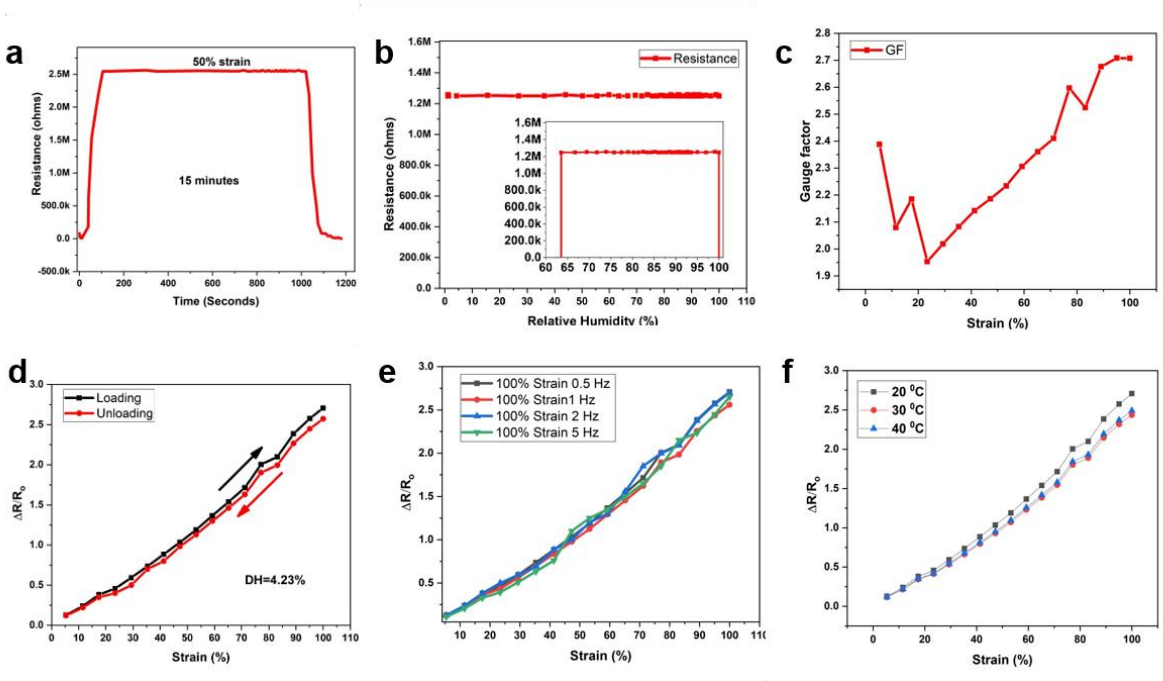

Figure 4-4 a) Resistance-Strain response of sensor from 0% to 100% strain and hysteresis behavior of device, b) Experimental results of resistance change ($\Delta R/R_0$) as a function of the applied frequency, c) Resistance response of sensor against applied tensile strain at three different temperatures, 20 ^{0}C, 30 ^{0}C, 40 ^{0}C. d) Sensor response in humidity controlled chamber from 0-100 %RH, e) gauge factor vs applied strain, f) stability analysis of sensor at 50% strain for ~15minutes

4.1.4 Cyclic Performance

The long-term stability of sensor was determined by applying cyclic stretching and relaxing at a speed of 0.5Hz. Device was loaded to 50% strain in each cycle and then released to 0% strain. The results were quite stable and endorse great level of tendency for reproducing the consistent response in various applications. *Figure 4-5* shows the relative resistance change of developed sensor against cyclic loading and unloading effect for 8000 cycles. It can be seen in figure 4a, the response is highly stable and nearly maintained constant base resistance. *Figure 4-5* b-c shows the first and last 10 cycles respectively which were zoomed and directly plotted from *Figure 4-5*a. Overall sensor's output is highly durable to a large number of cycles. This consistency also recommends the device to be a favorable candidate for robotics applications we normally operate for indefinitely high number of

cycles. For the commercialization of any device, it is very important that the designed device must possess high level of reproducibility. We tested three samples with same design and environmental parameters. The response of three samples are shown in *Figure 4-5*d, that clearly depicts a minute level of difference in resistance change when all sensors were stretched from 0% to 100% strain. All the performance parameters are summarized in *Table 1* along with recently reported sensors based on conductive liquid.

Table 1 Summary of performance results of recently reported fluidic stretchable strain sensors based on conductive liquid materials.

Sensing Material	**Stretchable Substrate**	**Strain**	**Strain Speed**	**DH**	**Gauge Factor**	**No. of Cycles**	**Optimization through Simulation**	**Ref.**
GaInSn	PDMS	50%	--	--	--	20	No	[116]
NaCl -Ecoflex	Ecoflex	50%	--	21.34%	--	--	No	[84]
Carbon grease ink	Ecoflex	100%	--	9.04%	3.8	1000	No	[117]
KI-Gly	Ecoflex	50%	2 Hz	5.3%	2.2	4000	No	[73]
ethylene glycol/NaCl	Ecoflex	250%	--	6.52%	<4	3000	Yes	[94]
Graphene/ Glycerin	Ecoflex	1000 %	--	--	45	10000	No	[118]
reduced graphene oxide/DI	Ecoflex	400%	--	31.6%	--	--	No	[119]
KCL-Gly	Ecoflex	100%	5 Hz	4.23%	2.7	8000	Yes	This Work

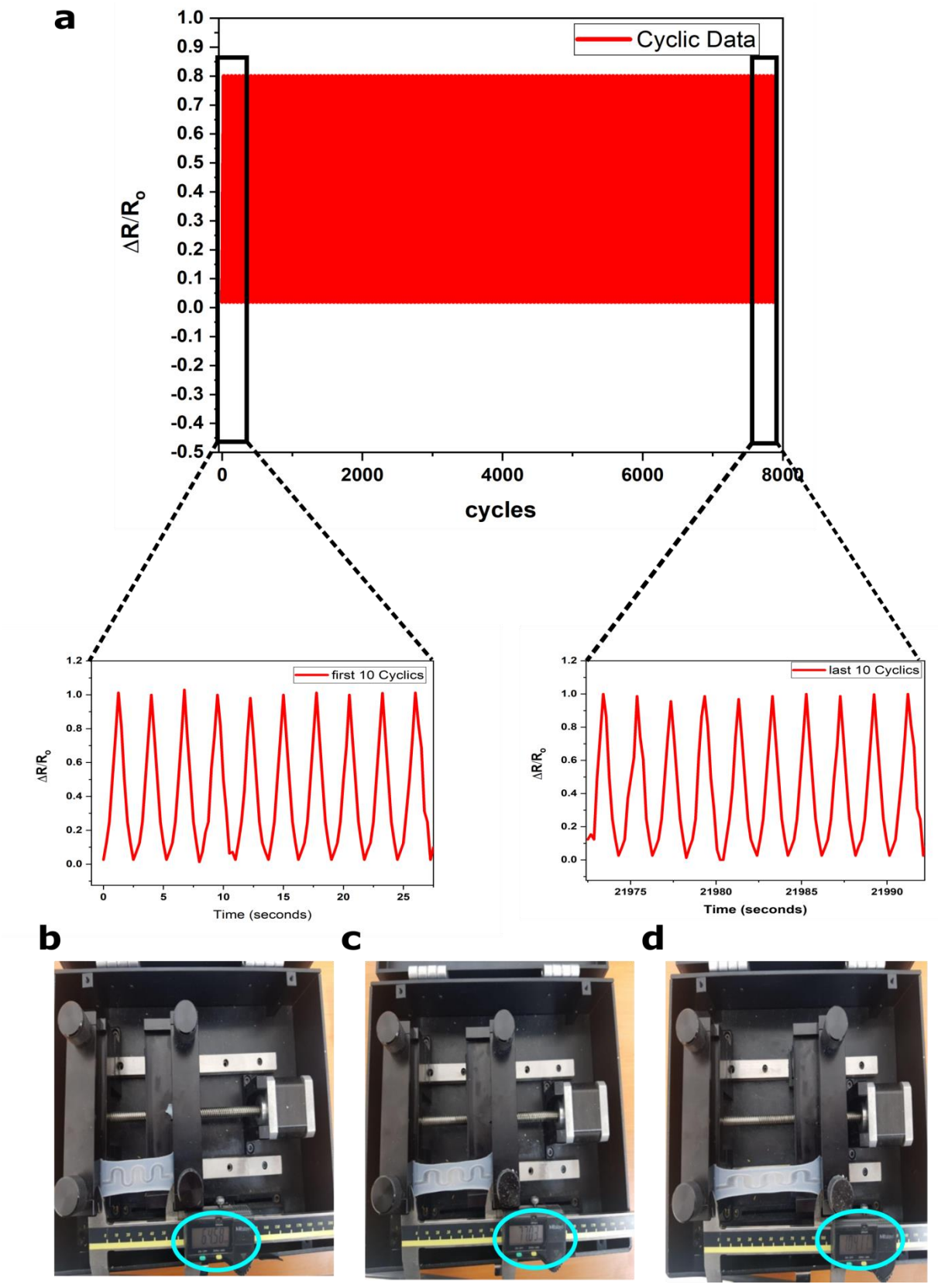

Figure 4-5 Cyclic Stretching and relaxing of sensor for 8000 cycles. a) Showing 8000 cycle's resistance response. b) Showing first 10 cycles resistance vs time. c) Last 10 cycle's resistance vs time, d-f) stills captured form a video at different strain levels

4.1.5 Sensor Applications

Finally the fabricated sensing device was used in three versatile applications; feedback strain sensor for robotic use inside water and to monitor human activity. For the first application, a single-joint robotic arm was printed using a commercial 3D printer. Two parts of leg were 70mm and 90mm long, respectively. We mainly focused to mimic the frog's leg which is commonly made for toys. However, this does not limit the scope of application, as the sensor could be used arbitrarily for any application that requires feedback information. The total angular movement of fabricated leg was up to 30 degree, therefore we analyzed the response our sensor for multiple cycles on three different movements (10 degree, 20 degree and 30 degree). The entire leg with sensor properly attached to joint was then immersed inside water. The response was quite coherent with the movement as can be seen in *Figure 4-6*a. For the first two movements the relative change in resistance was in the range of 0.21 with no major change however the response substantially raised to two-fold when the movement of 30 degree was applied. It is obvious that the output of device is easily distinguishable to various movements which will not require any complex circuitry for the comparator which supports our fabricated sensor to be good candidate to be cost-effective and reliable solution for high end robotic feedback including under water applications. In *Figure 4-6*b, human activity of drinking water was monitored. The device was attached to the upper part of neck of subject using adhesive tapers on the two ends. The activity was monitored for about 15 seconds. The relative change of 0.35 was measured; moreover this activity was monitored multiple times due to high inconsistency in the drinking style of same subject, so the most lucid behavior in terms of resistive behavior is shown here. Inset images show real sensor attached with human neck while left being the zoomed still. The optical images of printed robotic arm and strain sensor attached with it are shown in *Figure 4-6*e-g. It can be seen that sensor was immersed in pot, full of water. It was made sure to put that of arm downward which had sensor aside so the sensor has continuous contact with water. This confirmed the use of proposed sensor to be used for under water applications. The proposed device was further used as a human finger movement sensor. The device was attached to the upper part of index finger. The movement was classified in to two speeds, normal and quick bending. The results shown in figure 6c represent the slow and fast bending cycles of a human finger. The response was measured in a room temperature with relative humidity

level of ~41%, moreover sensor's output is quite distinguishable with very negligible noisy effect that further confirms sensor's application in human motion detection as wearable electronic sensor.

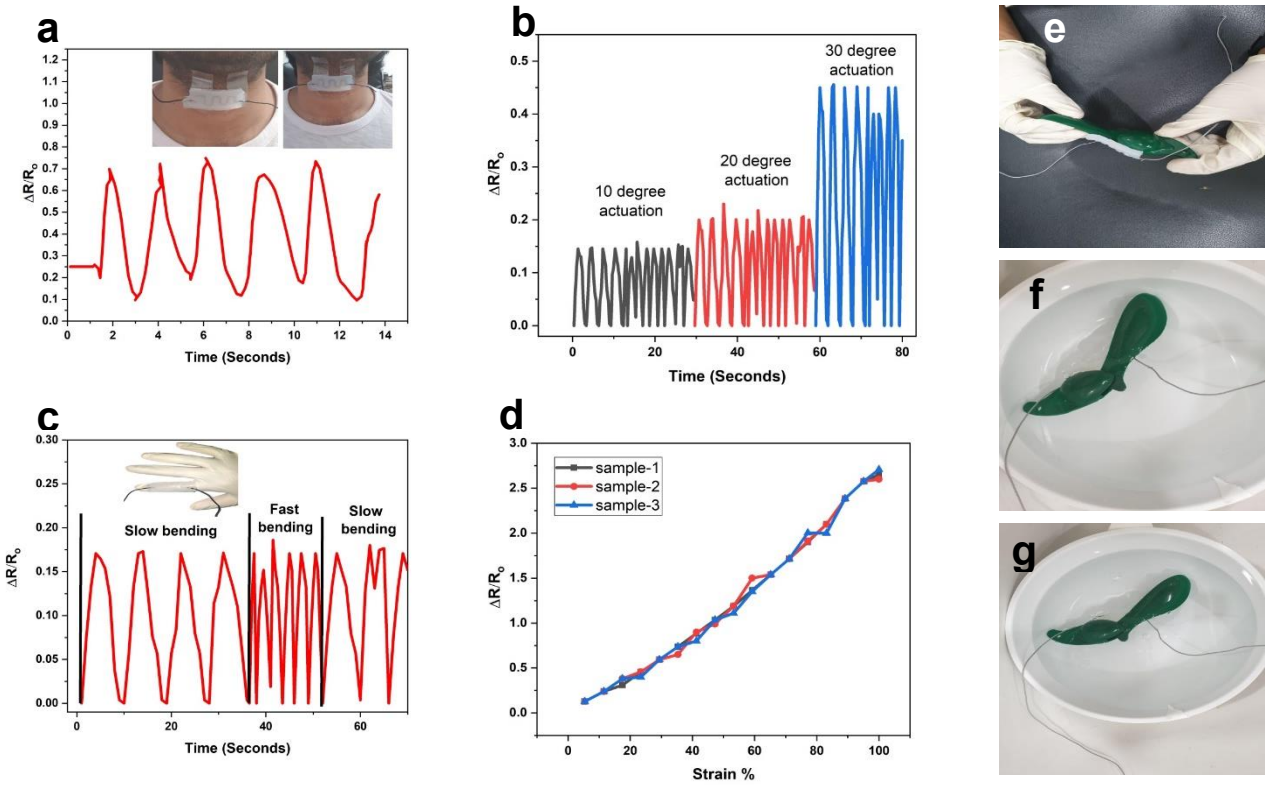

Figure 4-6 a) Resistance response of sensor attached with the joint of 3D printed robotic leg capable of rotation with angular displacement of 30 degree; response at 10 degree, 20 degree and 30 degree movement, b) sensor response in terms of relative resistance change to monitor the water drinking activity of human, c) bending response of sensor attached to human finger, d) reproducibility test of 3 samples e -g optical images of sensor attached with joint of arm in different states inside water.

4.2 Wrist Pulse Sensor

High performance biodegradable electronic devices are becoming popular due to their enormous applications as biomedical implants or short-term communication devices. They are biocompatible and eco-friendly. For example, wearable or implantable biodegradable pressure sensors are very useful for cardiovascular or blood flow monitoring. But unfortunately, very few previous research have focused on developing biodegradable pressure sensors. Here we propose a composite of Polylactic-co-glycolic acid (PLGA) and Polycaprolactone (PCL) for biodegradable piezo-capacitive pressure sensor fabrication for low pressure measurement in tactile ranges of ($0 < P < 5$ kPa). An electrospun PLGA-PCL composite membrane has been used as elastomeric dielectric sandwiched between two biodegradable iron-zinc (Fe-Zn) bilayer electrodes, deposited on degradable Polyvinyl alcohol (PVA) substrate using electron beam deposition, and encapsulated in PLGA thin films for device fabrication. PLGA-PCL nanofibrous dielectric membrane is highly compressible and porous having tunable mechanical as well as dielectric properties and has been reported first ever for biodegradable pressure sensor application. The sensitivity of the sensor was found to be 0.863 ± 0.025 kPa-1in the low pressure region ($0 < P \leq 1.86$ kPa) which is quite high as compared to previous literature on biodegradable sensors so far while it adapted to a value of 0.062 ± 0.005 kPa$-1$for high pressure region (1.86 kPa $< P \leq 4.6$ kPa). The lowest detected value was 1.24 Pa (at 10mgf). Sensor showed good average response and recovery times of 251 ms and 170 ms respectively. In vitro degradation studies of the sensor were performed in PBS solution and sensor lost 60% of its initial weight during first two weeks of degradation and continued to degrade even after that. After one week of incubation sensor showed a 19.5% decrease in low pressure measurement range while there was no significant difference in upper detection range. It has been used to measure the arterial pulse wave on wrist and a 4×4pressure sensor array was made to demonstrate its use in mapping different pressure points.

4.2.1 Sensor Fabrication

The commercially available 30 μm thick PVA sheet, after plasma treatment for 5 min to modify surface properties for electrodes deposition, was masked at the non-deposition area with inkjet-printed sticker paper readily available. After that a 10 nm thin layer of Fe followed by 100 nm layer of Zn was

deposited using the e-beam evaporation system to make bilayer electrodes onto the substrate. Thin layer of Fe was used to promote the adhesion between Zn electrodes and the main substrate. Moreover for the measurement of the pressor sensor, a custom made setup was used, as shown in *Figure 4-8*.

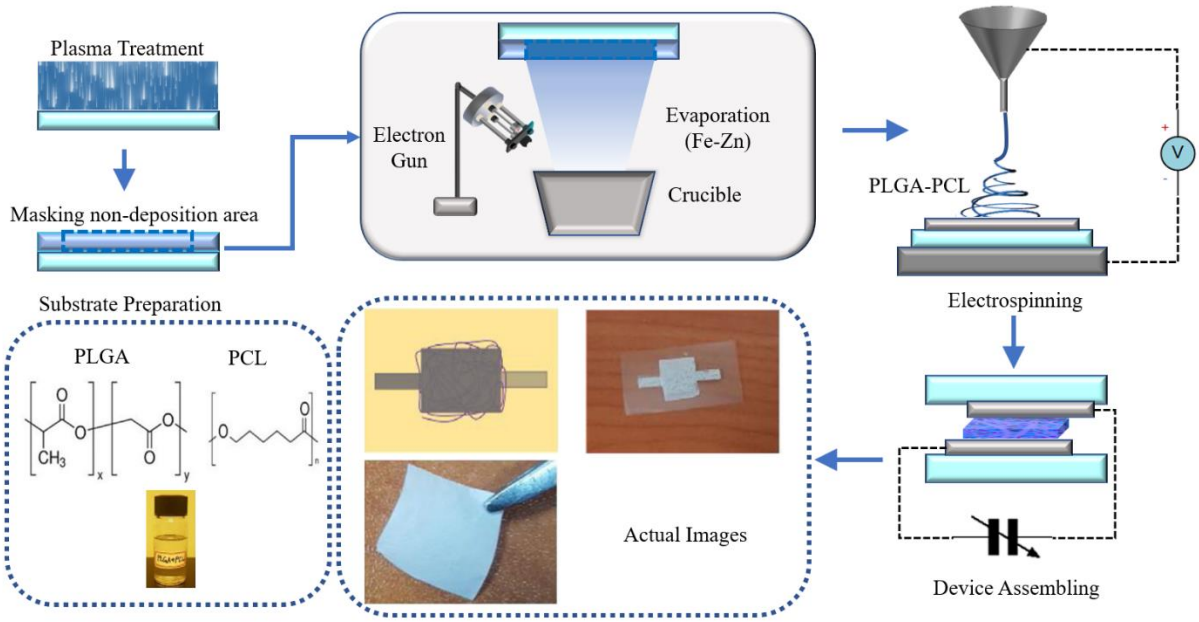

Figure 4-7 Step by step fabrication process of pressure sensor

Two as prepared electrode-substrate samples were used to make a sandwich like structure for the sensor later. For solution electrospinning of the dielectric material first a high viscosity ink of PLGA: PCL in 8:2was prepared in 2,2,2-Trifluroethanol. 0.8 g of PLGA and 0.2 g of PCL were dissolved in the 7.3 g of solvent and stirred magnetically for 6 h at 40◦C and 1500 rpm to form homogeneous solution. This ink formulation was chosen after comparing with 5:5 PLGA: PCL composition (which resulted in non-uniform fiber diameters, no performance improvement and could have possibly resulted in long degradation time of the composite membrane because of more PCL content). Then this high viscosity ink was used in electrospinning process (Applied Potential: 8.7 kV, Collector distance: 14 cm, Flow rate: 0.4 ml/hr) to form ~8 µm thick membrane of nanofibers and cut into 10mm*10 mm pieces as the composite biodegradable dielectric layer. After making electrical wiring connections, for

measurement, using silver epoxy to the electrodes the device was glued in a sandwich type structure after placing dielectric membrane using PVA solution as adhesive. At the end it was encapsulated using sping coating 5 µm thin layer of PLGA. The step by step fabrication process is shown in *Figure 4-7*.

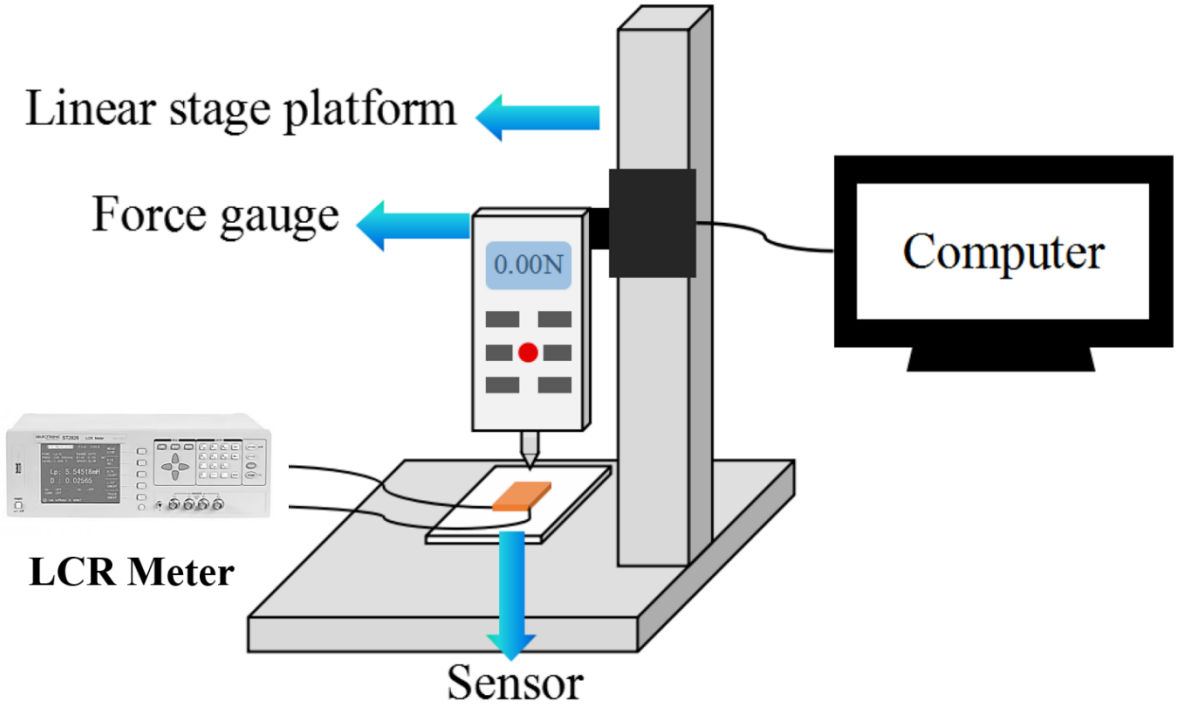

Figure 4-8 Custom made measurement setup for pressure sensor

4.2.2 Sensor Applications

An array of 4 × 4 pressure sensors was fabricated and utilized for demonstrating its use in spatial pressure distribution as shown in *Figure 4-9*. A commercially available pressure mapping platform along with their software was used to characterize the fabricated sensor array for this purpose. Different objects were placed on it to prove its usefulness in mapping pressure points.

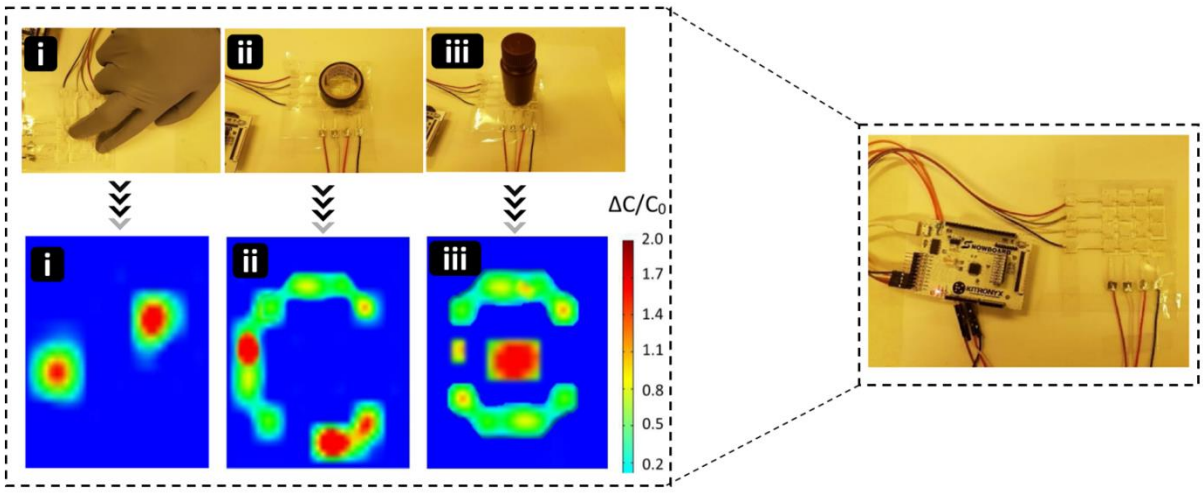

Figure 4-9 (a) 4 × 4 array prepared using dielectric membrane connected to commercially available pressure mapping platform, and Application of pressure (i) By using fingers (ii) By adhesive tape (iii) By a (powder) filled bottle, and their respective Snapshots of pressure profiles indicated in i, ii, iii taken from the software with scalebar showing relative change in capacitance with respect to color, whereas the rightmost picture shows the as-developed array and readout board.

As fabricated device was used to monitor the wrist pulse. For this purpose, a custom built setup using a 24bit capacitance to digital converter AD7746 was used along with an arduino micro-controller to record the capacitance data. The data was recorded at 40 Hz sampling frequency keeping in view the response and recovery times to produce minimum lag. The data for a normal pulse and pulse after 5 min of exercise were recorded to demonstrate the sensor's usefulness in vital monitoring. Sensor response for a 5 s interval has been shown in *Figure 4-10*. As can be seen in the figure that sensor is showing higher relative change in capacitance and higher frequency for pulse signal after 5 min of exercise because of the rise in blood pressure in wrist artery and in the heartbeat.

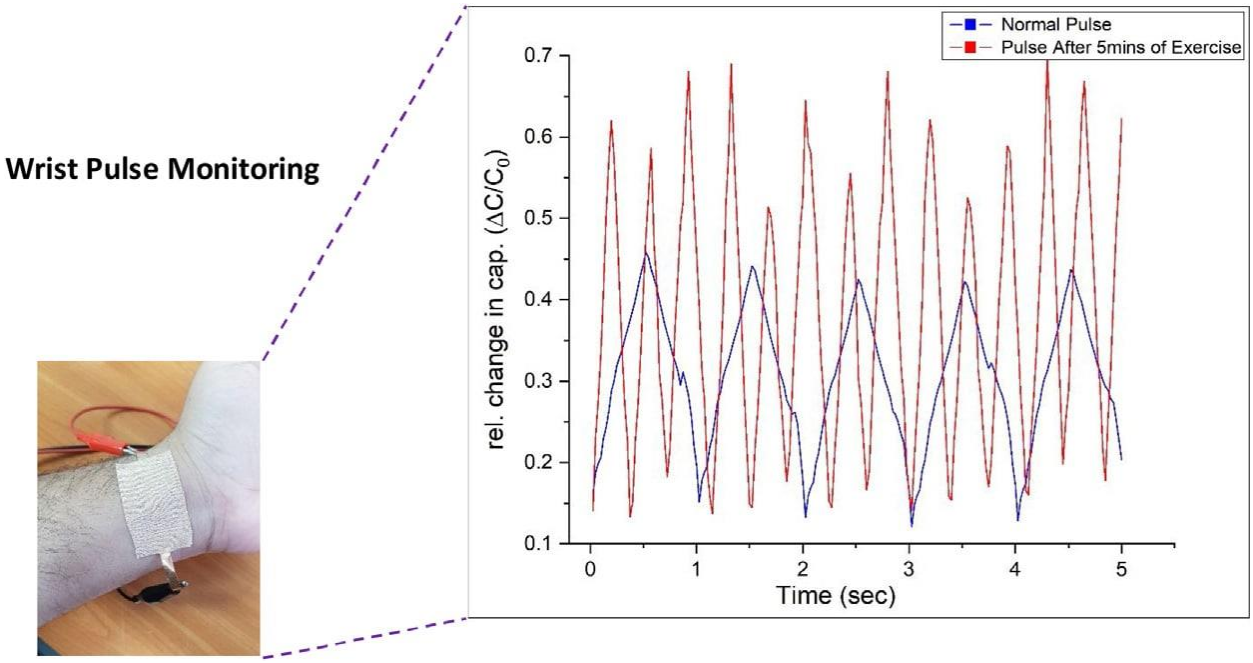

Figure 4-10 Wrist pulse rate measurement using custom made board

4.3 Soft Strain sensor based on PEDOT: PSS/MWCNTs

This research focuses on the design of a fluidic strain sensor based on a sinusoidal pattern filled with a novel biocompatible conductive poly(3,4-ethylenedioxythiophene) polystyrene sulfonate multiwall carbon nanotube (PEDOT:PSS/MWCNT) composite liquid. The presence of MWCNT further enhances the conductivity of the PEDOT:PSS solution, and the sensor. A two-order change in electrical resistance was observed across the electrodes of the developed sensor upon applying uniaxial strain of up to 150%. The sensor is fabricated using a simple process and exhibits high performance with hysteresis of 1.56%, considerably less than that of existing biocompatible solutions in addition to excellent sensitivity with a maximum GF of 89.4 at 150% strain. Moreover, the as-developed sensor achieves high linearity (R^2= 0.9935), stable cyclic performance for 1000 cycles at 30% strain, and the ability to follow the applied strain up to a maximum speed of 10 Hz. Moreover, the structure of the sensor is based on a sinusoidal pattern with 2.5 cycles, which was simulated in our previous study[120]. To confirm the device's performance under various environmental conditions, it was tested under the full range of humidity (0–100% RH) at various temperatures (20 ˚C–40 ˚C) using our in-house built electronically controlled chamber. As a proof-of-concept demonstration, the fabricated sensor was used with a single joint robotic leg as a high-end feedback sensor. Moreover, prior to using the sensor as a

wearable sensor, the biocompatibility of the device was tested by cell viability assessment of human epidermal keratinocytes HEKp and HUVEC. The simple fabrication process and ultrahigh sensitivity of the device make it a robust candidate for wearable and robotic applications.

4.3.1 Fabrication of Sensor

The fabrication of the fluidic strain sensor followed a two-step process. In the first step, an ultrastretchable elastomer, Ecoflex 00–30, was used. This material is commercially provided in two parts; A and B, which are mixed in an equal weight ratio (1:1). Prior to designing the elastomeric matrix, a mold containing a sinusoidal pattern was modeled using SolidWorks 13.0 and then 3D printed using a Creality CR20 printer by fused deposition modeling (FDM) as in our previous study. [5] The prepared Ecoflex solution was first mixed for 1 h, stirred, and then degassed. Before pouring the Ecoflex into the printed mold, two silicon-coated electrodes were attached. The solution present in the mold was cured for more than 4 h until it was fully cured, after which, it was carefully peeled off with great care so that the engraved channel was not damaged. A stable connection between the electrodes and the conductive liquid, and similarly with the measurement electronics, was of great importance, as a large strain such as 150% could break the electrical connection easily[17,94,121]; to resolve this problem, silicon-coated wires were used. This enabled the sensor to have a strong soft-to-rigid connection, improved the compatibility with the elastomeric matrix, and had minimum effect on the sensor's readouts. Moreover, the thickness variation was made in relation to gradient nature in the close vicinity of the electrodes; this further helped significantly improve the sensor's dimensional stability in the case of high-frequency strain applications. For the encapsulation of the sensor's pattern, a thin membrane was prepared by the blade-coating process. The membrane was half-cured, which took around 2 h at room temperature, and then it was bonded with an elastomeric matrix with a sinusoidal pattern. The pattern was fully encapsulated after bonding for 2 h. Moreover, the thickness of the membrane was kept in the range of 0.8–1.0 mm.

In the second step, the channel was filled with the liquid. However, with manual handling, two syringes from both ends could not fill the channel completely, leaving many bubbles that severely degraded

the sensor's sensing performance. Thus, a high synchronization between the two syringes was required, which was not possible with human handling. To make this possible, the syringes were actuated by stepper motors, which were controlled by an Arduino Mega. A program in C++ language was used to further calibrate the process. As a result, the conductive liquid was infilled using an automated process, and no bubbles were formed. However, owing to the filling of the channel, two tiny holes were created, which were closed using epoxy glue. *Figure 4-11* shows the sensor's design process.

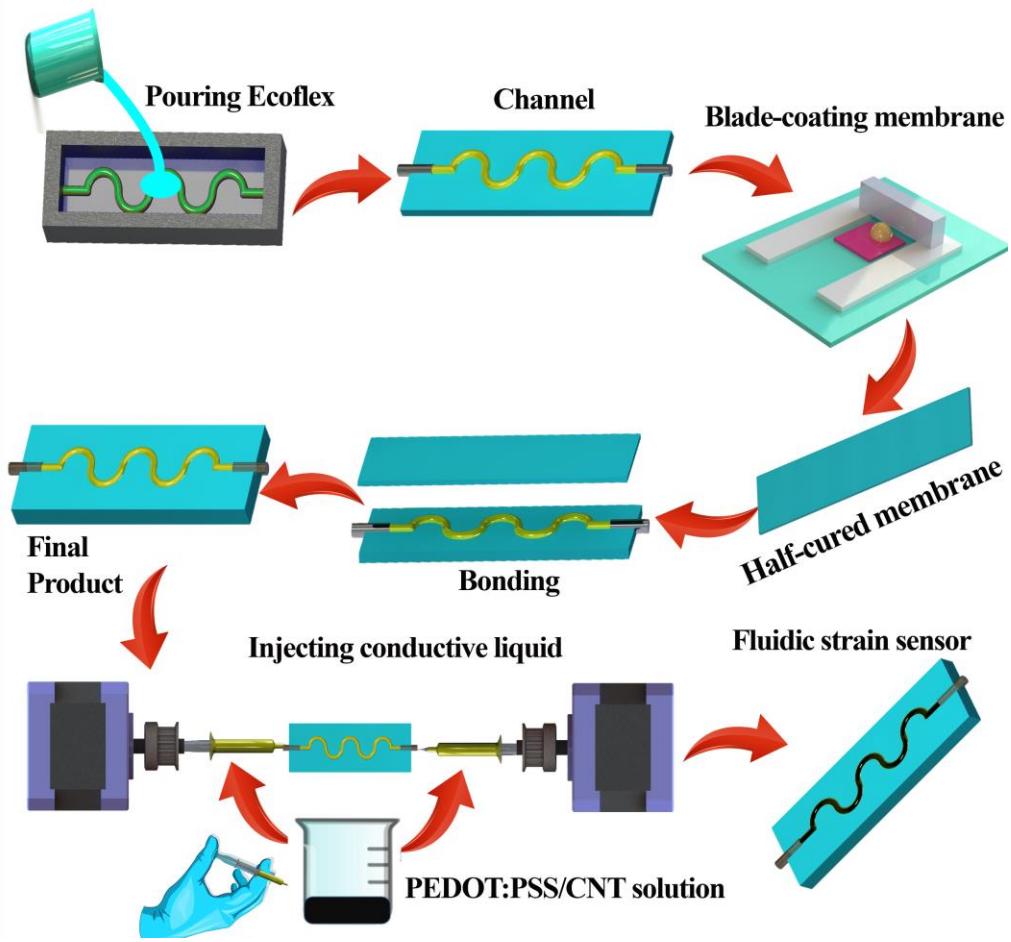

Figure 4-11 Step by Step Fabrication Process

4.3.2 Working Mechanism

The working principle of the proposed sensor is based on a simple concept[16,108,122,123]: the resistance is directly proportional to the effective length of the conductive liquid. Herein, as strain is applied to the device, its length starts increasing i.e., the length of the liquid leading to increased resistance across the two electrodes. The composite of PEDOT:PSS/MWCNT was used owing to its high shuttling capacity of electrons inside the channel, Moreover, for strain-sensing applications, it is important to

have a conductive polymer, which has the inherent feature of elasticity; PEDOT:PSS not only helps to minimize the hysteresis due to its faster conductive path recreations, but also retains the memory of its initial position at higher frequencies. The incorporation of MWCNT further improves the conductivity, sensitivity, and memory effect in addition to strengthening the conductive articulated paths between the electrodes. The structure of the conductive liquid present in the channel is shown in *Figure 4-12*(a). Moreover, the viscoelasticity of the elastomer also limits the ability of the sensors to achieve a better memory effect due to the imperfect attachment of the elastomer between sidewalls and conductive liquid molecules. This is a straight channel, wherein

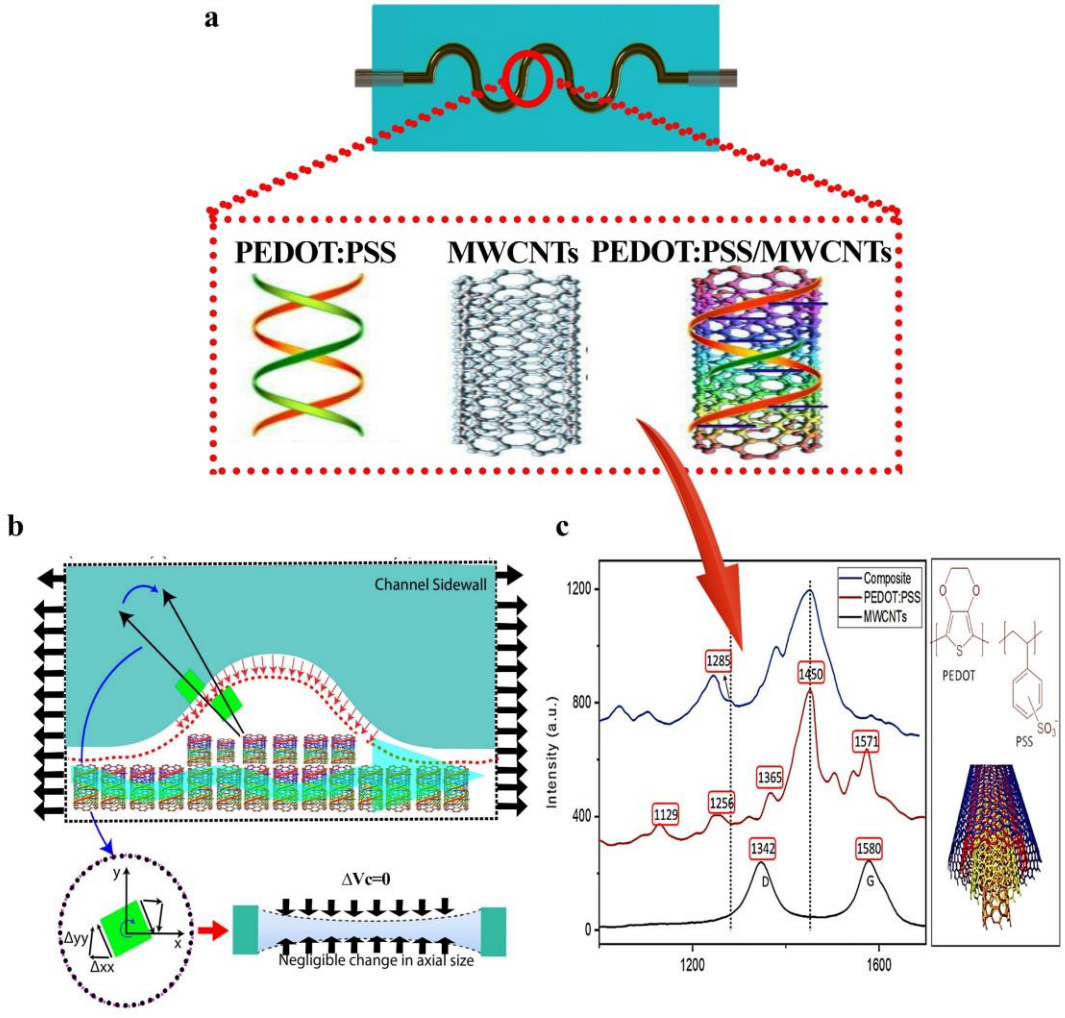

Figure 4-12 (a) Schematic showing structure of conductive PEDOT:PSS/MWCNT present in the channel. (b) Schematic showing a segment of the stretched sidewall of the infilled channel. Upon axial stretching, the effective length of the conductive liquid increases, whereas the relaxation is suppressed by the horizontal stress component. (c) Raman spectra of the composite of MWCNT and PEDOT:PSS, PEDOT:PSS, and the MWCNT.

the elastomer's volume (V_{EC}) increases owing to stretching. Moreover, the Poisson ratio of elastomers is lower than 0.5 in practice. However, in the proposed sensor, the volumes of the conductive liquid and elastomeric channel remain constant. To confirm the volume limitation (V_{EC}=V_{IL}), the channel is affected by compressing forces, enabling contraction in the axial direction. This contraction has been minimized by the design of the sinusoidal channel, which incorporates a sheer stress axial component and compressive force relaxation as can be seen in *Figure 4-12*(b); this causes significantly less lateral change in the length of the sensor. The non uniform strain–stress distribution in the wavy channel enables it to outperform as a simple straight channel[124–127]. *Figure 4-12*(c) shows the Raman spectra of the proposed composite and the individual MWCNT and PEDOT:PSS dispersions in DMF solvent (D, G, and 2D bands) at a resolution of 500 nm. Moreover, two functions were considered while performing the numerical analysis of the proposed strain sensor: the bulk relaxation modulus *K(t)* and the shear modulus *G(t)* as given in Eqs. (1) and (2), repectively. Herein, G_0 and K_0 represent the time-dependent shear modulus and bulk modulus, respectively, whereas the other parameters denote material coefficients[108,128–130].

$$K(t) = G_0 \sum_{i=1}^{n} g_i\left[\left(1 - e^{-t/\partial_i}\right)\right] \quad (1)$$

$$G(t) = K_0\left[1 - \sum_{i=1}^{n} k_i\left[\left(1 - e^{-t/\partial_i}\right)\right]\right] \quad (2)$$

4.3.3 Sensor's Electrical Response

The electrical characterization of the as-developed sensor was performed by measuring the output resistance across the two electrodes of the device against the applied uniaxial strain. The measured resistance was then converted into the relative change of resistance ($\Delta R/R_0 \times 100$). The sensor was tested in the strain range of 0–150%. *Figure 4-13* (a) shows the relative resistance against the applied strain of the sensor. The strain was increased/decreased with a speed of 0.5 Hz. Moreover, the hysteresis was calculated to be 1.56% using Eq. (1)[115,117,131,132]. There is significantly higher consistency among the curves for stretching and releasing, which is associated with the inherent elasticity of PEDOT:PSS and the unique sinusoidal design of the channel. The minimized memory effect in the proposed sensor makes it a robust option for use in high-end feedback and a myriad other relevant applications[118,133,134].

$$DH = \frac{A_{Loading} - A_{Unloading}}{A_{Loading}} \times 100 \quad (3)$$

It is essential that the strain sensor produces a consistent output resistance for various speed-driven strain applications[135–137]. To experimentally show that the strain sensor possesses this property, the uniaxial strain was applied over the full range (0–150%) at programmed speeds (0.5, 1, 2, 5, and 10 Hz), the results of which are shown in *Figure 4-13***.** The device under test showed excellent consistency when operated at different frequencies. Moreover, at all speeds, the GF was ~89.4. There was significant improvement in the performance of the proposed sensor at very low frequencies such as 0.5 Hz and at relatively high frequencies such as 10 Hz, which makes it a favorable candidate for not only human body motion quantification (which requires a frequency of 2 Hz) but also robotic applications (which can function at 10 Hz or more)[138]. Herein, the change in resistance and change in length are represented by ΔR and ΔL, and R_0 and L_0 represent the initial resistance and length respectively, when the sensor is under no strain condition. The sensor achieved a maximum GF of 89.4 at the maximum strain of 150%, which is considerably higher than that of fluidic strain sensors reported in the literature, as shown in Table 1. This ultrasensitive feature of the proposed sensor is due to the higher conductivity of the conductive liquid, the optimized design, and the strong electrical paths augmented by MWCNT. Moreover, there is some fluctuation in the GF response below 20% strain; this is due to the initial abrupt change in the viscoelastic strain/stress, which causes breakdown in the electrical paths. However, despite this fact, the minimum GF attained by the sensor was 55, which is itself a good performance figure of merit. Moreover the optical images of sensors under different bending states are shown in *Figure 4-14*.

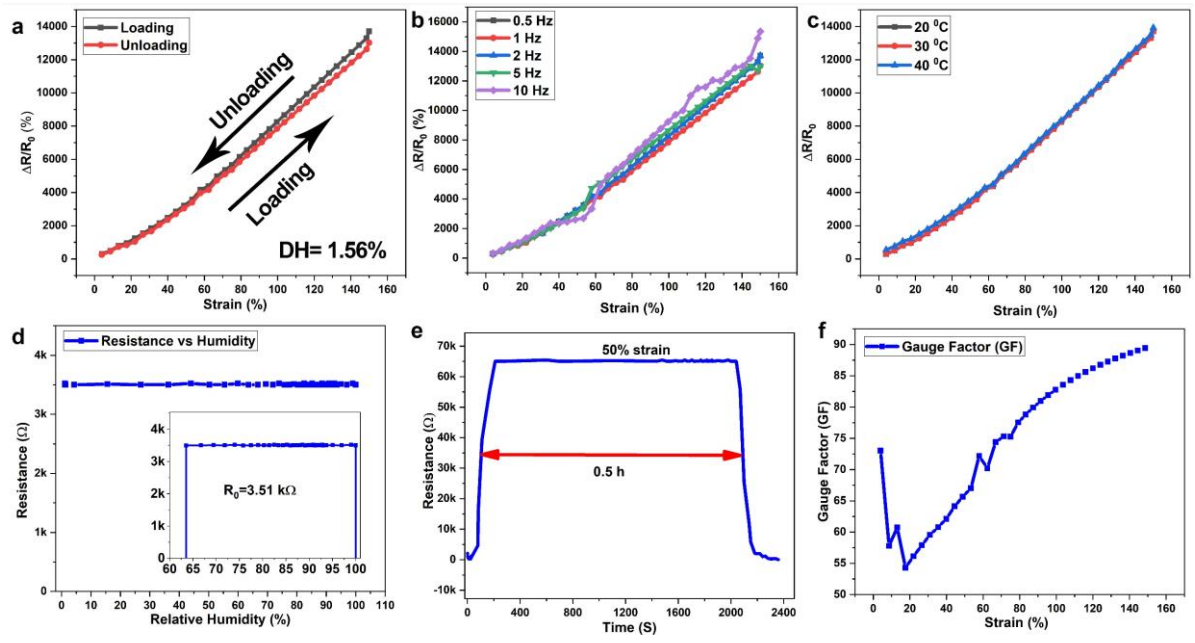

Figure 4-13 (a) Sensor loading/unloading response from 0 to 150 strain, (b) sensor response as a function of the applied frequency, c) sensor response at temperatures of 20, 30, and 40 ˚C. (d) sensor response under humid environment from 0–100 %RH, (e) sensor response at 50% strain for 0.5 h, and f) gauge factor plotted against applied strain.

The stability of the strain sensor plays a key role in high-end applications[139–141]. The higher the stability, the more precise and accurate the decisions that can be taken using the sensor's feedback. To confirm this, two different experiments were performed. First, a fixed strain of 50% was applied across the device for 0.5 h. The resistance was measured to be ~65 KΩ at a uniaxial strain of 50%; this remained constant throughout the experiment. Second, the device was tested for a long run (1000 cycles) at a strain of 30%. The speed during this experiment was fixed to be 0.5 Hz. Moreover, the proposed sensor is also compared with other fluidic strain sensors in *Table 2*.

Table 2 Comparison of proposed sensor with previously reported fluidic strain sensors.

Sensing Material	Matrix Material	Sensing Range	Strain Frequency	DH (%)	GF	Reproducibility	COD	Ref.
GaInSn	PDMS	50%	--	--	--	20	Almost linear	[142]
NaCl-Ecoflex	Ecoflex	50%	--	21.34 %	--	--	~0.999	[143]
Carbon grease solution	Ecoflex	100%	--	9.04 %	3.8	1000	Non-linear	[144]
KI-Gly	Ecoflex	50%	2 Hz	5.3%	2.2	4000	Almost linear	[110]

Ethylene glycol/NaCl	Ecoflex	250%	--	6.52 %	<4	3000	~0.989	[145]
PEDOT: PSS	PDMS	30%	--	~9%	12,000	--	--	[146]
Graphene/ Glycerine	Ecoflex	1000%	--	--	45	10,000	Almost linear	[119]
rGO/DI	Ecoflex	400%	--	31.6 %	--	--	Almost linear	[147]
KCL-Gly	Ecoflex	100%	5 Hz	4.23 %	2.7	8000	~0.99	[148]
PEDOT:PSS /MWCNT	Ecoflex	150%	10 Hz	1.56 %	89.4	1000	0.99	This work

4.3.4 Sensor's stability towards temperature and humidity

The stability of the sensor under humid conditions is essential; its response should not be affected by changes in atmospheric humidity[149,150]. To confirm the waterproof feature and stability under humid environment of the proposed fluidic strain sensor, we characterized its response over the entire range of relative humidity (0–100% RH) using our custom-designed computer-controlled chamber. For reference, a DTU-21D commercial sensor was used to measure the relative humidity, which was interfaced with an ESP232 board, and its data was serially logged to a computer, as shown in Fig. S3. The humidity of the chamber was gradually changed with the help of a proportional integrator and differentiator (PID) controller. It can be seen in *Figure 4-13* that the sensor's response is highly stable across the entire range of humidity. This implies that the proposed sensor is unaffected by environmental humidity conditions. Similarly, the fabricated device's performance was analyzed while changing the temperature. The sensor and custom-built stage were placed inside a temperature-controlled chamber in which the entire range of strain from 0 to 150% was applied. The experiment was performed at 20, 30, and 40 ˚C) and little effect of temperature on the proposed sensor was observed, indicating its stability for various wearable health-monitoring applications where the temperature is around 40 ˚C. This is also supported by the fact that the sensitivity of the sensor is not

dependent on the conductivity, i.e., the relative change in resistance is independent of the conductive solution.[34]

4.3.5 Reproducibility of Sensor

Figure 4-15 shows that the as-developed sensor achieved very fast response and recovery times of 720 and 900 ms, respectively. The rapid sensing performance of the sensor paves the way for its efficient use in high-speed robotic applications more efficiently. The relationships between resistance and GF is represented by Eq. (5), where γ represents the contact resistance.

$$\frac{\Delta R}{R_0} = \gamma(GF^2 + 2GF) \qquad (5)$$

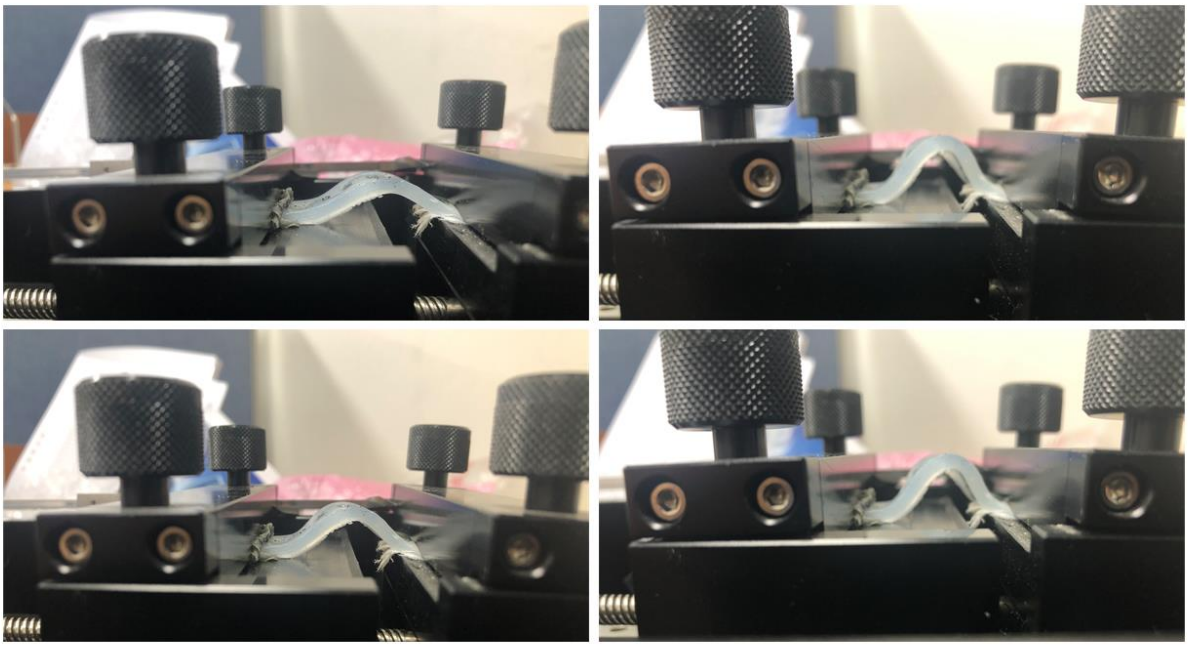

Figure 4-14 optical images of sensor in various physical bending states

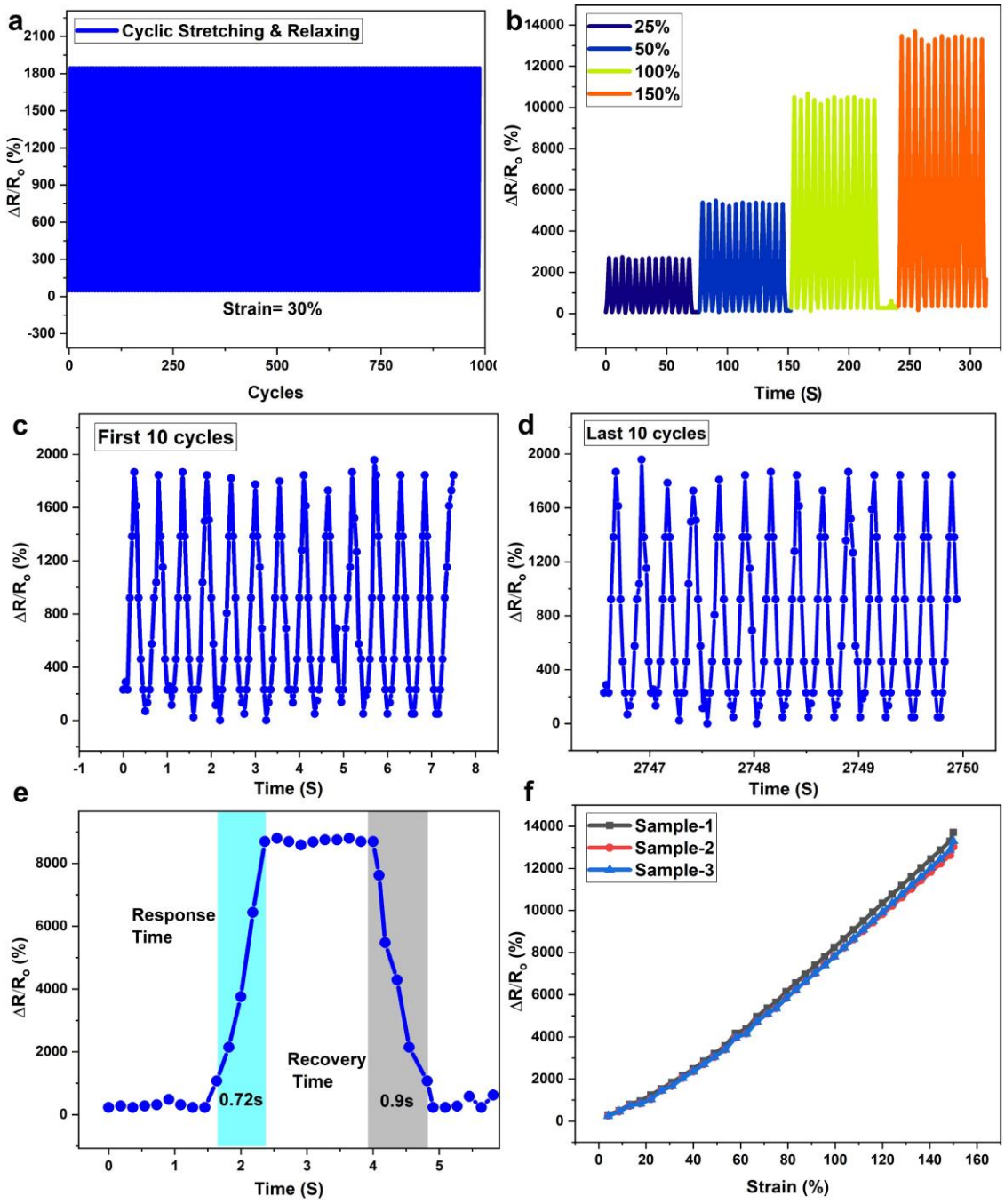

Figure 4-15 (a) Cyclic performance of sensor for 1000 cycles. (b) Stability for 10 cycles under different strains;(c) first 10 cycles, (d) last 10 cycles, (e) sensor response and recovery times, and (f) response of three different samples plotted against strain.

4.3.6 Sensor Biocompatibility Test

To target wearable applications for humans, it is of considerable importance that the proposed sensor must be biocompatible. This means that the sensor has not only high electrical and mechanical performance but also must not pose any harm to human skin when it is worn. To prove the biocompatibility of the developed sensor, we performed a live-dead assay experiment. For this,

human epidermal keratinocytes (HEKp)(Thermo Fisher scientific) human umbilical vein endothelial cells (HUVEC)

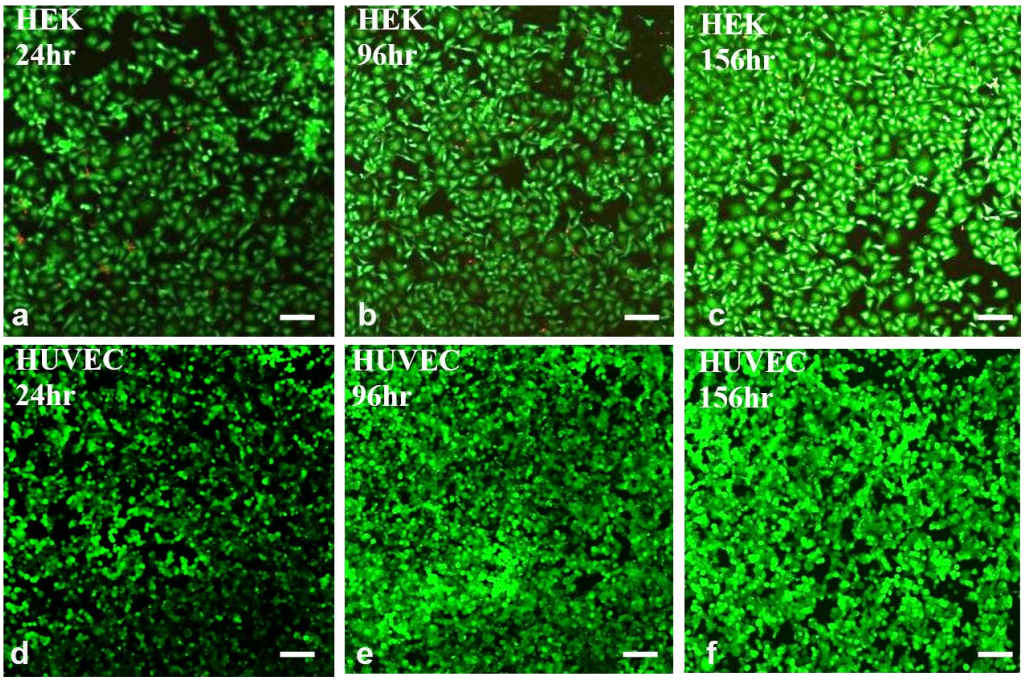

Figure 4-16(a) Confocal laser scanning microscopy z-stack images of HEKp increasing viability on the strain sensor after 48, 96, and 156 h. (Green fluorescence shows live cells, whereas red fluorescence shows dead cells, scale bar 100 µm (n=3), (b) Confocal laser scanning microscopy z-stack images of HUVEC cells showing increasing viability on strain sensor after 48, 96, and 156 h. (Green fluorescence shows live cells whereas red fluorescence shows dead cells; scale bar 100 µm (n=3).

(ATCC) were cultured on a sensor surface made of PDMS at passage numbers 4 and 5 respectively. HEkp were cultured in serum-free mediaEpiLife® media with 60 µM calcium and human keratinocyte growth supplement (HKGS), and HUVEC were cultured in vascular cell basal medium with growth factors. Sensors containing cells were placed in petri plates with different media and kept at 37 °C in 5% CO2 at 99% humidity for 7 days in incubator. Cell viability was determined by a lived/dead assay kit (Thermo fisher). After 48, 96, and 156 h, the sensors containing HEKp and HUVEC were washed with PBS and stained with 2 µl of calcein to stain the incubated live cells for 20 min at room temperature and with 0.5 µl of ethidium homodimer to stain the dead cells for 10 min at room temperature. They were then washed thrice and visualized under a confocal laser scanning microscope. Z-stack images were taken for all the samples.

4.3.7 Sensor Applications

The fabricated sensor was used in different wearable electronics and robotic applications for the measurement of human body motion and angle measurement, respectively. In the first proof-of-

concept demonstration, the fabricated device was attached to the upper side of the index finger of a human's right hand using adhesive bandages, while thin and lightweight electrical wires were used to read out the device's electrical resistance. The subject was free to bend the finger as desired. The experiment was divided into two movements: slow bending and fast bending. Moreover, before the data-logging process, it was ensured that the output resistance of the sensor was stable (~3.51 KΩ). *Figure 4-17* shows the results of the movement of the finger at room temperature and normal humidity (~40%). Slow bending and fast bending are clearly distinguishable, further confirming that the sensor's response effectively follows the motion of the human finger. As soon as the finger is bent, the relative change in resistance jumps to a value of around 300%. Similarly, it is important to monitor the mechanical movement of the human arm, especially in the case of fracture. To target this application, the device was wrapped around the elbow, which was at the center of the sensor. The data logged by the LCR meter is shown in *Figure 4-17*. Similarly to the experiment on the finger, the subject was instructed to freely move his elbow at either a normal speed or a high speed as desired. The sensor showed response of 590% and 10% in the bending and straightening conditions, respectively. The as-developed fluidic strain sensor clearly distinguished the two movements without any unit of pre-calibration or pretreatment. Moreover, to prove that the proposed sensor can measure small changes in physical deformations, the device was attached to the middle of the subject's neck. The subject was asked to drink water and the electrical response of the strain sensor was measured in real time, as shown in. Herein, the relative change in resistance (6–30%) clearly indicates the drinking style of the subject. Moreover, the proposed device is promising for studying human drinking styles for various liquids.

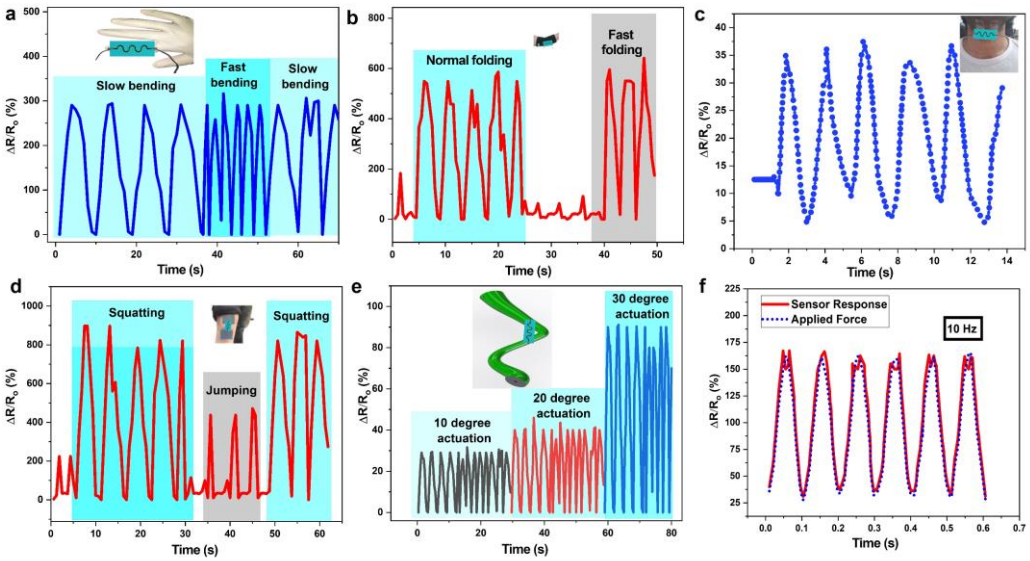

Figure 4-17 (a) Monitoring of man finger motion, (b) sensor response when attached on human elbow joint (c) monitoring of water drinking pattern, (d) sensor response when attached on knee joint, (e) sensor response when used with 3D-printed robotic leg, and (f) sensor response when strain with a speed of 10 Hz is applied.

Finally, the sensor was used as a high-end feedback sensor for a robotic leg. For this, a leg mimicking that of a frog was 3D-printed using a commercial printer. An Ultraflex PLA filament was used to print the soft leg of the frog. The actuation of the leg was made possible by embedding shape memory alloy (SMA) functional wires (0.3 mm diameter). Upon the application of voltage (5 V), a current of around 1 A started flowing, which heated the wires, resulting in the contraction of the leg. However, to optimise the performance of the sensor to the leg, three angular movements (10, 20 and 30˚) of the leg were precalibrated using electrical-current optimization methods. *Figure 4-17*(e) shows the response of the sensor to the movements over multiple cycles. The device's response is highly distinguishable for each movement. The change in electrical resistance at 30˚ actuation was more than double at 10˚ actuation. The actuation speed was limited by the cooling/heating of the SMA-embedded robotic leg. However, to further prove that the device can even be used for relatively high frequency applications in robotics, we applied a sinusoidally governed strain to the custom-made stage used to uniaxially deform the fabricated device at two frequencies (5 and 10 Hz). The responses of the sensor at 5 and 10 Hz are given in *Figure 4-17* and *Figure 4-17*(f), respectively. The device closely follows the applied sinusoidal pattern of the strain at the very higher frequency of 10 Hz. This proves that the proposed sensor can be a robust option for high-end robotic feedback application, in addition to personal wearable electronics.

5 Conclusion and Future Work

The main focus of this research work was to develop high performance soft sensing devices using 3D printing and Reverse Offset Printing. The targeted sensors include environmental monitoring sensor (humidity sensor) and (strain and humidity sensors) and fluidic strain sensors (for body posture detection and robotics high-end feedback applications) have been developed with successful target of enhancing the features like sensing capacity, detection range, detection limit, cyclic stability, hysteresis, data reproducibility, robustness, transient response time, linearity and accuracy. Using inter-disciplinary research including materials science, processes, printing systems, sensing principle and device physics, the targets were achieved. The developed sensors are easy to be interfaced and even simple read-out circuits can be used to use the sensors. The key conclusions of the research and the possible future work can be summarized as:

1. A biocompatible humidity sensor has been developed using a poly lactic glycolic acid (PLGA) as a sensing layer for the first time using all printing methods with excellent performance parameters that are comparable to commercial devices.
2. The best performance parameters achieved for the humidity sensor were full range of sensing (0 – 100% RH), fast response time of 3 s, recovery time of 6 s, highly linear response (0.9810 ROC), stability up to 5 mm radius bendability, high reproducibility and a very good choice for human breathing activity monitoring.
3. A fluidic based strain sensor based on a novel biocompatible ionic liquid composed of potassium chloride and glycerol and optimized structure was developed using a very simple and cost-effective fabrication method.
4. The soft strain sensor showed excellent results such as sensitivity up to 100% uniaxial strain, low hysteresis of 4.23%, consistent response up to 5 Hz speed, Gauge Factor for 2.7, high cyclic performance on 8000 cycles, temperature resistant up to 40 °C and fully waterproof.
5. Another ultra flexible, highly stable, and linear fluidic strain sensor using a biocompatible conductive composite based on PEDOT:PSS/MWCNT was fabricated which showed excellent

performance parameters that are better or at least comparable to the existing liquid based strain sensors in the literature.

6. The developed strain sensor showed excellent sensitivity up to 150% uniaxial stretching and relaxation, minimum hysteresis (1.56%), high linearity (R^2= 0.9935), sensitivity with a GF of 89.4 at 150% strain, high level of reproducibility for 1000 cycle, consistency in response up to at a speed of 10 Hz, temperature and humidity resistant and feature of biocompatibility.
7. The future target is to focus more number of applications while simultaneously decreasing the fabrication cost and significantly enhancing the scalability of the developed sensors. In case of application-specific sensors, some parameters can be compromised on the cost of some very important parameters. The aim is to optimize the sensing devices' structure and working mechanism using analytical mathematics and rigorous simulation work in addition to proposing novel biocompatible materials. To achieve all these goals, inter-disciplinary research is a fundamental key. The current research focuses on the design high performance small-sized sensors and embedding them into soft robots for targeting environmental exploration applications. Moreover, high-throughput multi-array sensors will also be used in various scenarios in future.

Declaration

I (Afaque Manzoor), hereby declare that this thesis entitled "**Design and Fabrication of Soft Sensors for Wearable Electronics and Robotics Applications**", submitted to Jeju National University in the partial fulfillment of the requirements for the award of the **Degree of Doctor of Philosophy** in the department **of Mechatronics Engineering** is a record of original and independent research work done and published by during the period March 2018 to February 2021 under the supervision of the **Professor Kyung Hyung Choi.** This thesis work is based on the publications in reputed journals and it has not been formed for the award of any other Degree/Diploma/Associateship/Fellowship to any individual of any university.

Afaque Manzoor

References

(1) Choi, K. H.; Kim, H. B.; Ali, K.; Sajid, M.; Uddin Siddiqui, G.; Chang, D. E.; Kim, H. C.; Ko, J. B.; Dang, H. W.; Doh, Y. H. Hybrid Surface Acoustic Wave- Electrohydrodynamic Atomization (SAW-EHDA) for the Development of Functional Thin Films. *Sci. Rep.* **2015**, *5* (March), 1–14. https://doi.org/10.1038/srep15178.

(2) Saleem, M.; Ahmed, N.; Tahir, M. M.; Zahid, M. S.; Sajid, M.; Bashir, M. M.; Road, W. EFFECT OF HUMIDITY ON THE NiPc BASED ORGANIC PHOTO FIELD EFFECT. **2016**, *17* (1), 84–89.

(3) Sauerbrunn, E.; Chen, Y.; Didion, J.; Yu, M.; Smela, E.; Bruck, H. A. Thermal Imaging Using Polymer Nanocomposite Temperature Sensors. *Phys. Status Solidi* **2015**, *212* (10), 2239–2245. https://doi.org/10.1002/pssa.201532114.

(4) Gerwen, P. Van. Nanoscaled Interdigitated Electrode Arrays for Biochemical Sensors. *Sensors Actuators B Chem.* **1998**, *49*, 73–80. https://doi.org/10.1109/SENSOR.1997.635249.

(5) Duan, D. Nanozyme-Strip for Rapid Local Diagnosis of Ebola. *Biosens. Bioelectron.* **2015**, *74*, 134–141. https://doi.org/10.1016/j.bios.2015.05.025.

(6) Nidzworski, D. Universal Biosensor for Detection of Influenza Virus. *Biosens. Bioelectron.* **2014**, *59*, 239–242. https://doi.org/10.1016/j.bios.2014.03.050.

(7) Andreescu. Trends and Challenges in Biochemical Sensors for Clinical and Environmental Monitoring*. *Pure Appl. Chem* **2004**, *76* (4), 861–878. https://doi.org/10.1351/pac200476040861.

(8) Shavanova, K. Application of 2D Non-Graphene Materials and 2D Oxide Nanostructures for Biosensing Technology. *Sensors (Switzerland)* **2016**, *16* (2), 1–23. https://doi.org/10.3390/s16020223.

(9) Varghese, S. Two-Dimensional Materials for Sensing: Graphene and Beyond. *Electronics* **2015**, *4* (3), 651–687. https://doi.org/10.3390/electronics4030651.

(10) Sajid, M.; Kim, H. B.; Yang, Y. J.; Jo, J.; Choi, K. H. Highly Sensitive BEHP-Co-MEH:PPV+ Poly(Acrylic Acid) Partial Sodium Salt Based Relative Humidity Sensor. *Sensors Actuators, B Chem.* **2017**, *246*, 809–818. https://doi.org/10.1016/j.snb.2017.02.162.

(11) Soomro, A. M.; Jabbar, F.; Ali, M.; Lee, J.-W.; Mun, S. W.; Choi, K. H. All-Range Flexible and Biocompatible Humidity Sensor Based on Poly Lactic Glycolic Acid (PLGA) and Its Application in Human Breathing for Wearable Health Monitoring. *J. Mater. Sci. Mater. Electron.* **2019**, *30* (10). https://doi.org/10.1007/s10854-019-01277-1.

(12) Choi, K. H.; Sajid, M.; Aziz, S.; Yang, B.-S. Wide Range High Speed Relative Humidity Sensor Based on PEDOT:PSS–PVA Composite on an IDT Printed on Piezoelectric Substrate. *Sensors Actuators A Phys.* **2015**, *228*, 40–49. https://doi.org/10.1016/j.sna.2015.03.003.

(13) Soomro, A. M.; Jabbar, F.; Ali, M.; Lee, J.-W.; Mun, S. W.; Choi, K. H. All-Range Flexible and Biocompatible Humidity Sensor Based on Poly Lactic Glycolic Acid (PLGA) and Its Application in Human Breathing for Wearable Health Monitoring. *J. Mater. Sci. Mater. Electron.* **2019**, *30* (10). https://doi.org/10.1007/s10854-019-01277-1.

(14) Soomro, A. M.; Khalid, M. A. U.; Shah, I.; Kim, S. W.; Kim, Y. S.; Choi, K. H. Highly Stable Soft Strain Sensor Based on Gly-KCl Filled Sinusoidal Fluidic Channel for Wearable and Water-Proof Robotic Applications. *Smart Mater. Struct.* **2020**, *29* (2). https://doi.org/10.1088/1361-665X/ab540b.

(15) Shah, I.; Aziz, S.; Soomro, A. M.; Kim, K.; Kim, S. W.; Choi, K. H. Numerical and Experimental Investigation of Y-Shaped Micromixers with Mixing Units Based on Cantor Fractal Structure for Biodiesel Applications. *Microsyst. Technol.* **2020**, *9*. https://doi.org/10.1007/s00542-020-05036-9.

(16) Khalid, M. A. U.; Kim, S. W.; Lee, J.; Soomro, A. M.; Rehman, M. M.; Lee, B. G.; Choi, K. H. Resistive Switching Device Based on SrTiO3/PVA Hybrid Composite Thin Film as Active Layer. *Polymer (Guildf).* **2020**, *189* (January), 122183. https://doi.org/10.1016/j.polymer.2020.122183.

(17) Lee, J. W.; Soomro, A. M.; Waqas, M.; Khalid, M. A. U.; Choi, K. H. A Highly Efficient Surface Modified Separator Fabricated with Atmospheric Atomic Layer Deposition for High Temperature Lithium Ion Batteries. *Int. J. Energy Res.* **2020**, No. December 2019, 1–12. https://doi.org/10.1002/er.5371.

(18) Ali, M.; Kim, Y. S.; Khalid, M. A. U.; Soomro, A. M.; Lee, J. W.; Lim, J. H.; Choi, K. H.; Ho, L. S. On-Chip Real-Time Detection and Quantification of Reactive Oxygen Species in MCF-7 Cells through an in-House Built Fluorescence Microscope. *Microelectron. Eng.* **2020**, *233* (July), 111432. https://doi.org/10.1016/j.mee.2020.111432.

(19) Jabbar, F.; Soomro, A. M.; Lee, J.; Ali, M.; Kim, Y. S.; Lee, S.; Choi, K. H. Robust Fluidic Biocompatible Strain Sensor Based on PEDOT : PSS / CNT Composite for Human-Wearable and High-End Robotic Applications. **2020**, *32* (12), 1–17.

(20) Sajid, M.; Aziz, S.; Kim, G. B.; Kim, S. W.; Jo, J.; Choi, K. H. Bio-Compatible Organic Humidity Sensor Transferred to Arbitrary Surfaces Fabricated Using Single-Cell-Thick Onion Membrane

as Both the Substrate and Sensing Layer. *Sci. Rep.* **2016**. https://doi.org/10.1038/srep30065.

(21) Soomro, A. M.; Shah, M. A. Higher Order MIMO System Capacity Assessment Using Singular Value Decomposition While Considering Power Constraint Problem. *Bahria Univ. J. Inf. Commun. Technol.* **2015**, *8* (2), 65–69.

(22) Jiang, P.; Yu, D.; Zhang, W.; Mao, Z.; Gao, C. Influence of Bovine Serum Albumin Coated Poly(Lactic-Co-Glycolic Acid) Particles on Differentiation of Mesenchymal Stem Cells. *RSC Adv.* **2015**, *5* (51), 40924–40931. https://doi.org/10.1039/c5ra07219k.

(23) Amin, R.; Islam, S. H.; Biswas, G. P.; Khan, M. K.; Kumar, N. A Robust and Anonymous Patient Monitoring System Using Wireless Medical Sensor Networks. *Futur. Gener. Comput. Syst.* **2018**, *80*, 483–495. https://doi.org/10.1016/j.future.2016.05.032.

(24) Sagade, A. A.; Sharma, R. Copper Sulphide (CuxS) as an Ammonia Gas Sensor Working at Room Temperature. *Sensors Actuators, B Chem.* **2008**, *133* (1), 135–143. https://doi.org/10.1016/j.snb.2008.02.015.

(25) Boudaden, J.; Steinmaßl, M.; Endres, H. E.; Drost, A.; Eisele, I.; Kutter, C.; Müller-Buschbaum, P. Polyimide-Based Capacitive Humidity Sensor. *Sensors (Switzerland)* **2018**, *18* (5), 1220–1223. https://doi.org/10.3390/s18051516.

(26) Liakos, I. L.; Mondini, A.; Filippeschi, C.; Mattoli, V.; Tramacere, F.; Mazzolai, B. Towards Ultra-Responsive Biodegradable Polysaccharide Humidity Sensors. *Mater. Today Chem.* **2017**, *6*, 1–12. https://doi.org/10.1016/j.mtchem.2017.08.001.

(27) Kuang, Q.; Lao, C.; Wang, Z. L.; Xie, Z.; Zheng, L. JACS127_6070(2007)_High-Sesitivity Humidity Sensor Based on a Single SnO2 NW.Pdf. **2007**, 6070–6071.

(28) Mutee ur Rehman, M.; Muqeet Rehman, M.; Sajid, M.; Lee, J. W.; Na, K. H.; Ko, J. B.; Choi, K. H. Significance of Encapsulating Organic Temperature Sensors through Spatial Atmospheric Atomic Layer Deposition for Protection against Humidity. *J. Mater. Sci. Mater. Electron.* **2018**, *29* (17), 14396–14405. https://doi.org/10.1007/s10854-018-9572-4.

(29) Takeda, Y.; Yoshimura, Y.; Shiwaku, R.; Hayasaka, K.; Sekine, T.; Okamoto, T.; Matsui, H.; Kumaki, D.; Katayama, Y.; Tokito, S. Organic Complementary Inverter Circuits Fabricated with Reverse Offset Printing. *Adv. Electron. Mater.* **2018**, *4* (1), 5–9. https://doi.org/10.1002/aelm.201700313.

(30) Li, Y.; Deng, C.; Yang, M. A Novel Surface Acoustic Wave-Impedance Humidity Sensor Based on the Composite of Polyaniline and Poly(Vinyl Alcohol) with a Capability of Detecting Low

Humidity. *Sensors Actuators, B Chem.* **2012**, *165* (1), 7–12. https://doi.org/10.1016/j.snb.2011.12.037.

(31) Chethan, B.; Ravikiran, Y. T.; Vijayakumari, S. C.; Rajprakash, H. G.; Thomas, S. Nickel Substituted Cadmium Ferrite as Room Temperature Operable Humidity Sensor. *Sensors Actuators, A Phys.* **2018**, *280*, 466–474. https://doi.org/10.1016/j.sna.2018.08.017.

(32) Qu, W.; Wlodarski, W.; Meyer, J.-U. Comparative Study on Micromorphology and Humidity Sensitive Properties of Thin-Film and Thick-Film Humidity Sensors Based on Semiconducting MnWO 4. *Sensors Actuators B* **2000**, *64*, 76–82. https://doi.org/http://dx.doi.org/10.1016/S0925-4005(99)00487-6.

(33) Zhou, G.; Byun, J. H.; Oh, Y.; Jung, B. M.; Cha, H. J.; Seong, D. G.; Um, M. K.; Hyun, S.; Chou, T. W. Highly Sensitive Wearable Textile-Based Humidity Sensor Made of High-Strength, Single-Walled Carbon Nanotube/Poly(Vinyl Alcohol) Filaments. *ACS Appl. Mater. Interfaces* **2017**, *9* (5), 4788–4797. https://doi.org/10.1021/acsami.6b12448.

(34) Najeeb, M. A.; Ahmad, Z.; Shakoor, R. A. Organic Thin-Film Capacitive and Resistive Humidity Sensors: A Focus Review. *Adv. Mater. Interfaces* **2018**, *5* (21), 1–19. https://doi.org/10.1002/admi.201800969.

(35) Zhao, J.; Li, N.; Yu, H.; Wei, Z.; Liao, M.; Chen, P.; Wang, S.; Shi, D.; Sun, Q.; Zhang, G. Highly Sensitive MoS2Humidity Sensors Array for Noncontact Sensation. *Adv. Mater.* **2017**, *29* (34), 1–7. https://doi.org/10.1002/adma.201702076.

(36) Sajid, M.; Siddiqui, G. U.; Kim, S. W.; Na, K. H.; Choi, Y. S.; Choi, K. H. Thermally Modified Amorphous Polyethylene Oxide Thin Films as Highly Sensitive Linear Humidity Sensors. *Sensors Actuators, A Phys.* **2017**, *265*, 102–110. https://doi.org/10.1016/j.sna.2017.08.040.

(37) Takeda, Y.; Yoshimura, Y.; Shiwaku, R.; Hayasaka, K.; Sekine, T.; Okamoto, T.; Matsui, H.; Kumaki, D.; Katayama, Y.; Tokito, S. Organic Complementary Inverter Circuits Fabricated with Reverse Offset Printing. *Adv. Electron. Mater.* **2018**, *4* (1), 1700313. https://doi.org/10.1002/aelm.201700313.

(38) Li, H. Y.; Lee, C. S.; Kim, D. H.; Lee, J. H. Flexible Room-Temperature NH3 Sensor for Ultrasensitive, Selective, and Humidity-Independent Gas Detection. *ACS Appl. Mater. Interfaces* **2018**, *10* (33), 27858–27867. https://doi.org/10.1021/acsami.8b09169.

(39) Leonardi, S. G.; Wlodarski, W.; Li, Y.; Donato, N.; Sofer, Z.; Pumera, M.; Neri, G. A Highly Sensitive Room Temperature Humidity Sensor Based on 2D-WS2 Nanosheets. *FlatChem* **2018**, *9* (January), 21–26. https://doi.org/10.1016/j.flatc.2018.05.001.

(40) Lee, J.; Mulmi, S.; Thangadurai, V.; Park, S. S. Magnetically Aligned Iron Oxide/Gold Nanoparticle-Decorated Carbon Nanotube Hybrid Structure as a Humidity Sensor. *ACS Appl. Mater. Interfaces* **2015**, *7* (28), 15506–15513. https://doi.org/10.1021/acsami.5b03862.

(41) Reynolds, A. J.; Conboy, J. C. Barium Titanate Nanoparticle Based Nonlinear Optical Humidity Sensor. *Sensors Actuators, B Chem.* **2018**, *273* (June), 921–926. https://doi.org/10.1016/j.snb.2018.07.004.

(42) Kim, H. B.; Sajid, M.; Kim, K. T.; Na, K. H.; Choi, K. H. Linear Humidity Sensor Fabrication Using Bi-Layered Active Region of Transition Metal Carbide and Polymer Thin Films. *Sensors Actuators, B Chem.* **2017**, *252*, 725–734. https://doi.org/10.1016/j.snb.2017.06.052.

(43) Strangfeld, C.; Kruschwitz, S. Monitoring of the Absolute Water Content in Porous Materials Based on Embedded Humidity Sensors. *Constr. Build. Mater.* **2018**, *177*, 511–521. https://doi.org/10.1016/j.conbuildmat.2018.05.044.

(44) Varghese, O. K.; Kichambre, P. D.; Gong, D.; Ong, K. G.; Dickey, E. C.; Grimes, C. A. Gas Sensing Characteristics of Multi-Wall Carbon Nanotubes. *Sensors Actuators, B Chem.* **2001**, *81* (1), 32–41. https://doi.org/10.1016/S0925-4005(01)00923-6.

(45) Yusop, A. H. M.; Daud, N. M.; Nur, H.; Kadir, M. R. A.; Hermawan, H. Controlling the Degradation Kinetics of Porous Iron by Poly(Lactic-Co-Glycolic Acid) Infiltration for Use as Temporary Medical Implants. *Sci. Rep.* **2015**, *5* (May), 1–17. https://doi.org/10.1038/srep11194.

(46) Ali, S.; Hassan, A.; Hassan, G.; Bae, J.; Lee, C. H. All-Printed Humidity Sensor Based on Gmethyl-Red/Methyl-Red Composite with High Sensitivity. *Carbon N. Y.* **2016**, *105*, 23–32. https://doi.org/10.1016/j.carbon.2016.04.013.

(47) Zheng, Q.; Zou, Y.; Zhang, Y.; Liu, Z.; Shi, B.; Wang, X.; Jin, Y.; Ouyang, H.; Li, Z.; Wang, Z. L. Biodegradable Triboelectric Nanogenerator as a Life-Time Designed Implantable Power Source. *Sci. Adv.* **2016**, *2* (3), 1–10. https://doi.org/10.1126/sciadv.1501478.

(48) Noh, M. S.; Kim, S.; Hwang, D. K.; Kang, C. Y. Self-Powered Flexible Touch Sensors Based on PZT Thin Films Using Laser Lift-Off. *Sensors Actuators, A Phys.* **2017**, *261*, 288–294. https://doi.org/10.1016/j.sna.2017.04.046.

(49) Siddiqui, G. U.; Sajid, M.; Ali, J.; Kim, S. W.; Doh, Y. H.; Choi, K. H. Wide Range Highly Sensitive Relative Humidity Sensor Based on Series Combination of MoS2and PEDOT:PSS Sensors Array. *Sensors Actuators, B Chem.* **2018**, *266*, 354–363. https://doi.org/10.1016/j.snb.2018.03.134.

(50) Meeus, J.; Scurr, D. J.; Amssoms, K.; Davies, M. C.; Roberts, C. J.; Van Den Mooter, G. Surface Characteristics of Spray-Dried Microspheres Consisting of PLGA and PVP: Relating the Influence of Heat and Humidity to the Thermal Characteristics of These Polymers. *Mol. Pharm.* **2013**, *10* (8), 3213–3224. https://doi.org/10.1021/mp400263d.

(51) Navale, S. T.; Mane, A. T.; Chougule, M. A.; Shinde, N. M.; Kim, J.; Patil, V. B. Highly Selective and Sensitive CdS Thin Film Sensors for Detection of NO2 Gas. *RSC Adv.* **2014**, *4* (84), 44547–44554. https://doi.org/10.1039/c4ra06531j.

(52) Xiao, X.; Zhang, Q. J.; He, J. H.; Xu, Q. F.; Li, H.; Li, N. J.; Chen, D. Y.; Lu, J. M. Polysquaraines: Novel Humidity Sensor Materials with Ultra-High Sensitivity and Good Reversibility. *Sensors Actuators, B Chem.* **2018**, *255*, 1147–1152. https://doi.org/10.1016/j.snb.2017.04.069.

(53) Jawad, H. M.; Nordin, R.; Gharghan, S. K.; Jawad, A. M.; Ismail, M. Energy-Efficient Wireless Sensor Networks for Precision Agriculture: A Review. *Sensors (Switzerland)* **2017**, *17* (8). https://doi.org/10.3390/s17081781.

(54) Sajid, M.; Dang, H. W.; Na, K. H.; Choi, K. H. Highly Stable Flex Sensors Fabricated through Mass Production Roll-to-Roll Micro-Gravure Printing System. *Sensors Actuators, A Phys.* **2015**, *236*, 73–81. https://doi.org/10.1016/j.sna.2015.10.037.

(55) Sun, L.; Wang, B.; Wang, Y. A Novel Silicon Carbide Nanosheet for High-Performance Humidity Sensor. *Adv. Mater. Interfaces* **2018**, *5* (6), 1–9. https://doi.org/10.1002/admi.201701300.

(56) Challeton, C.; Branea, F.; Schlumberger, M.; Gaillard, N.; De Vathaire, F.; Badie, C.; Antonini, P.; Parmentier, C. Characterization and Radiosensitivity at High or Low Dose Rate of Four Cell Lines Derived from Human Thyroid Tumors. *Int. J. Radiat. Oncol. Biol. Phys.* **1997**, *37* (1), 163–169. https://doi.org/10.1021/acsami.8b07373.

(57) Bobo, D.; Robinson, K. J.; Islam, J.; Thurecht, K. J.; Corrie, S. R. Nanoparticle-Based Medicines: A Review of FDA-Approved Materials and Clinical Trials to Date. *Pharm. Res.* **2016**, *33* (10), 2373–2387. https://doi.org/10.1007/s11095-016-1958-5.

(58) Miao, J.; Cai, L.; Zhang, S.; Nah, J.; Yeom, J.; Wang, C. Air-Stable Humidity Sensor Using Few-Layer Black Phosphorus. *ACS Appl. Mater. Interfaces* **2017**, *9* (11), 10019–10026. https://doi.org/10.1021/acsami.7b01833.

(59) Torsi, L.; Dodabalapur, A.; Cioffi, N.; Sabbatini, L.; Zambonin, P. G. NTCDA Organic Thin-Film-Transistor as Humidity Sensor: Weaknesses and Strengths. *Sensors Actuators, B Chem.* **2001**, *77* (1–2), 7–11. https://doi.org/10.1016/S0925-4005(01)00664-5.

(60) Yang, Y. J.; Kim, H. C.; Sajid, M.; Kim, S.; Aziz, S.; Choi, Y. S.; Choi, K. H. Drop-on-Demand Electrohydrodynamic Printing of High Resolution Conductive Micro Patterns for MEMS Repairing. *Int. J. Precis. Eng. Manuf.* **2018**, *19* (6), 811–819. https://doi.org/10.1007/s12541-018-0097-9.

(61) Trung, T. Q.; Lee, N. E. Flexible and Stretchable Physical Sensor Integrated Platforms for Wearable Human-Activity Monitoringand Personal Healthcare. *Adv. Mater.* **2016**, *28* (22), 4338–4372. https://doi.org/10.1002/adma.201504244.

(62) Yu, H. W.; Kim, H. K.; Kim, T.; Bae, K. M.; Seo, S. M.; Kim, J. M.; Kang, T. J.; Kim, Y. H. Self-Powered Humidity Sensor Based on Graphene Oxide Composite Film Intercalated by Poly(Sodium 4-Styrenesulfonate). *ACS Appl. Mater. Interfaces* **2014**, *6* (11), 8320–8326. https://doi.org/10.1021/am501151v.

(63) Sajid, M.; Kim, H. B.; Lim, J. H.; Choi, K. H. Liquid-Assisted Exfoliation of 2D HBN Flakes and Their Dispersion in PEO to Fabricate Highly Specific and Stable Linear Humidity Sensors. *J. Mater. Chem. C* **2018**, *6* (6), 1421–1432. https://doi.org/10.1039/c7tc04933a.

(64) Smith, A. D.; Elgammal, K.; Niklaus, F.; Delin, A.; Fischer, A. C.; Vaziri, S.; Forsberg, F.; Råsander, M.; Hugosson, H.; Bergqvist, L.; Schröder, S.; Kataria, S.; Östling, M.; Lemme, M. C. Resistive Graphene Humidity Sensors with Rapid and Direct Electrical Readout. *Nanoscale* **2015**, *7* (45), 19099–19109. https://doi.org/10.1039/c5nr06038a.

(65) Cheng, B.; Tian, B.; Xie, C.; Xiao, Y.; Lei, S. Highly Sensitive Humidity Sensor Based on Amorphous Al2O3nanotubes. *J. Mater. Chem.* **2011**, *21* (6), 1907–1912. https://doi.org/10.1039/c0jm02753g.

(66) Zhao, Y.; Yang, B.; Liu, J. Effect of Interdigital Electrode Gap on the Performance of SnO2-Modified MoS2capacitive Humidity Sensor. *Sensors Actuators, B Chem.* **2018**, *271* (May), 256–263. https://doi.org/10.1016/j.snb.2018.05.084.

(67) Rehman, M. M.; Siddiqui, G. U.; Doh, Y. H.; Choi, K. H. Highly Flexible and Electroforming Free Resistive Switching Behavior of Tungsten Disulfide Flakes Fabricated through Advanced Printing Technology. *Semicond. Sci. Technol.* **2017**, *32* (9). https://doi.org/10.1088/1361-6641/aa77db.

(68) Dumitru, A. C.; Espinosa, F. M.; Garcia, R.; Foschi, G.; Tortorella, S.; Valle, F.; Dallavalle, M.; Zerbetto, F.; Biscarini, F. In Situ Nanomechanical Characterization of the Early Stages of Swelling and Degradation of a Biodegradable Polymer. *Nanoscale* **2015**, *7* (12), 5403–5410. https://doi.org/10.1039/c5nr00265f.

(69) Jiang, K.; Zhao, H.; Dai, J.; Kuang, D.; Fei, T.; Zhang, T. Excellent Humidity Sensor Based on LiCl Loaded Hierarchically Porous Polymeric Microspheres. *ACS Appl. Mater. Interfaces* **2016**, *8* (38), 25529–25534. https://doi.org/10.1021/acsami.6b08071.

(70) Ponnusamy, T.; Lawson, L. B.; Freytag, L. C.; Blake, D. A.; Ayyala, R. S.; John, V. T. In Vitro Degradation and Release Characteristics of Spin Coated Thin Films of PLGA with a "Breath Figure" Morphology. *Biomatter* **2012**, *2* (2), 77–86. https://doi.org/10.4161/biom.20390.

(71) Vivekananthan, V.; Alluri, N. R.; Purusothaman, Y.; Chandrasekhar, A.; Selvarajan, S.; Kim, S. J. Biocompatible Collagen Nanofibrils: An Approach for Sustainable Energy Harvesting and Battery-Free Humidity Sensor Applications. *ACS Appl. Mater. Interfaces* **2018**, *10* (22), 18650–18656. https://doi.org/10.1021/acsami.8b02915.

(72) Tiefenauer, R. F.; Dalgaty, T.; Keplinger, T.; Tian, T.; Shih, C. J.; Vörös, J.; Aramesh, M. Monolayer Graphene Coupled to a Flexible Plasmonic Nanograting for Ultrasensitive Strain Monitoring. *Small* **2018**, *14* (28), 1–7. https://doi.org/10.1002/smll.201801187.

(73) Xu, S.; Vogt, D. M.; Hsu, W.-H.; Osborne, J.; Walsh, T.; Foster, J. R.; Sullivan, S. K.; Smith, V. C.; Rousing, A. W.; Goldfield, E. C.; Wood, R. J. Biocompatible Sensors: Biocompatible Soft Fluidic Strain and Force Sensors for Wearable Devices (Adv. Funct. Mater. 7/2019). *Adv. Funct. Mater.* **2019**, *29* (7), 1970038. https://doi.org/10.1002/adfm.201970038.

(74) Wang, Y.; Gong, S.; Wang, S. J.; Simon, G. P.; Cheng, W. Volume-Invariant Ionic Liquid Microbands as Highly Durable Wearable Biomedical Sensors. *Mater. Horizons* **2016**, *3* (3), 208–213. https://doi.org/10.1039/c5mh00284b.

(75) Cheng, Y.; Wang, R.; Sun, J.; Gao, L. A Stretchable and Highly Sensitive Graphene-Based Fiber for Sensing Tensile Strain, Bending, and Torsion. *Adv. Mater.* **2015**, *27* (45), 7365–7371. https://doi.org/10.1002/adma.201503558.

(76) Ahmad, J.; Andersson, H.; Sidén, J. Screen-Printed Piezoresistive Sensors for Monitoring Pressure Distribution in Wheelchair. *IEEE Sens. J.* **2019**, *19* (6), 2055–2063. https://doi.org/10.1109/JSEN.2018.2885638.

(77) Lin, Y.; Gordon, O.; Khan, M. R.; Vasquez, N.; Genzer, J.; Dickey, M. D. Vacuum Filling of Complex Microchannels with Liquid Metal. *Lab Chip* **2017**, *17* (18), 3043–3050. https://doi.org/10.1039/c7lc00426e.

(78) Tong, R.; Chen, G.; Pan, D.; Qi, H.; Li, R.; Tian, J.; Lu, F.; He, M. Highly Stretchable and Compressible Cellulose Ionic Hydrogels for Flexible Strain Sensors. *Biomacromolecules* **2019**, acs.biomac.9b00322. https://doi.org/10.1021/acs.biomac.9b00322.

(79) Costa, J. C.; Spina, F.; Lugoda, P.; Garcia-Garcia, L.; Roggen, D.; Münzenrieder, N. Flexible Sensors—From Materials to Applications. *Technologies* **2019**, *7* (2), 35. https://doi.org/10.3390/technologies7020035.

(80) Dickey, M. D.; Chiechi, R. C.; Larsen, R. J.; Weiss, E. A.; Weitz, D. A.; Whitesides, G. M. Eutectic Gallium-Indium (EGaIn): A Liquid Metal Alloy for the Formation of Stable Structures in Microchannels at Room Temperature. *Adv. Funct. Mater.* **2008**, *18* (7), 1097–1104. https://doi.org/10.1002/adfm.200701216.

(81) Gao, Q.; Li, H.; Zhang, J.; Xie, Z.; Zhang, J.; Wang, L. Microchannel Structural Design For a Room-Temperature Liquid Metal Based Super-Stretchable Sensor. *Sci. Rep.* **2019**, *9* (1), 1–8. https://doi.org/10.1038/s41598-019-42457-7.

(82) Liang, X.; Cheong, H.; Chui, C. K.; Yeow, C.-H. A Fabric-Based Wearable Soft Robotic Limb. *J. Mech. Robot.* **2019**, 1. https://doi.org/10.1115/1.4043024.

(83) Ali, A.; Hantanasirisakul, K.; Abdala, A.; Urbankowski, P.; Zhao, M. Q.; Anasori, B.; Gogotsi, Y.; Aïssa, B.; Mahmoud, K. A. Effect of Synthesis on Performance of MXene/Iron Oxide Anode Material for Lithium-Ion Batteries. *Langmuir* **2018**, *34* (38), 11325–11334. https://doi.org/10.1021/acs.langmuir.8b01953.

(84) Russo, S.; Ranzani, T.; Liu, H.; Nefti-Meziani, S.; Althoefer, K.; Menciassi, A. Soft and Stretchable Sensor Using Biocompatible Electrodes and Liquid for Medical Applications. *Soft Robot.* **2015**, *2* (4), 146–154. https://doi.org/10.1089/soro.2015.0011.

(85) Herrmann, J.; Müller, K. H.; Reda, T.; Baxter, G. R.; Raguse, B.; De Groot, G. J. J. B.; Chai, R.; Roberts, M.; Wieczorek, L. Nanoparticle Films as Sensitive Strain Gauges. *Appl. Phys. Lett.* **2007**, *91* (18), 1–4. https://doi.org/10.1063/1.2805026.

(86) Yoon, S. G.; Koo, H. J.; Chang, S. T. Highly Stretchable and Transparent Microfluidic Strain Sensors for Monitoring Human Body Motions. *ACS Appl. Mater. Interfaces* **2015**, *7* (49), 27562–27570. https://doi.org/10.1021/acsami.5b08404.

(87) Bhattacharjee, M.; Soni, M.; Escobedo, P.; Dahiya, R. PEDOT:PSS Microchannel-Based Highly Sensitive Stretchable Strain Sensor. *Adv. Electron. Mater.* **2020**. https://doi.org/10.1002/aelm.202000445.

(88) Qin, L.; Liang, X.; Huang, H.; Chui, C. K.; Yeow, R. C.-H.; Zhu, J. A Versatile Soft Crawling Robot with Rapid Locomotion. *Soft Robot.* **2019**, *00* (00), soro.2018.0124. https://doi.org/10.1089/soro.2018.0124.

(89) Wan, J.; Wang, Q.; Zang, S.; Huang, X.; Wang, T.; Liu, G.; Li, C.; Ren, X. Highly Stretchable and Sensitive Liquid-Type Strain Sensor Based on a Porous Elastic Rope/Elastomer Matrix Composite Structure. *Compos. Sci. Technol.* **2019**, *182* (June), 107707. https://doi.org/10.1016/j.compscitech.2019.107707.

(90) Deng, J.; Zhuang, W.; Bao, L.; Wu, X.; Gao, J.; Wang, B.; Sun, X.; Peng, H. A Tactile Sensing Textile with Bending-Independent Pressure Perception and Spatial Acuity. *Carbon N. Y.* **2019**, *149*, 63–70. https://doi.org/10.1016/j.carbon.2019.04.019.

(91) Yang, G.; Pang, G.; Pang, Z.; Gu, Y.; Mantysalo, M.; Yang, H. Non-Invasive Flexible and Stretchable Wearable Sensors with Nano-Based Enhancement for Chronic Disease Care. *IEEE Rev. Biomed. Eng.* **2019**, *12*, 34–71. https://doi.org/10.1109/RBME.2018.2887301.

(92) Kang, J.; Tok, J. B.-H.; Bao, Z. Self-Healing Soft Electronics. *Nat. Electron.* **2019**. https://doi.org/10.1038/s41928-019-0235-0.

(93) Amjadi, M.; Yoon, Y. J.; Park, I. Ultra-Stretchable and Skin-Mountable Strain Sensors Using Carbon Nanotubes-Ecoflex Nanocomposites. *Nanotechnology* **2015**, *26* (37), 375501. https://doi.org/10.1088/0957-4484/26/37/375501.

(94) Choi, D. Y.; Kim, M. H.; Oh, Y. S.; Jung, S. H.; Jung, J. H.; Sung, H. J.; Lee, H. W.; Lee, H. M. Highly Stretchable, Hysteresis-Free Ionic Liquid-Based Strain Sensor for Precise Human Motion Monitoring. *ACS Appl. Mater. Interfaces* **2017**, *9* (2), 1770–1780. https://doi.org/10.1021/acsami.6b12415.

(95) Yeo, J. C.; Yu, J.; Koh, Z. M.; Wang, Z.; Lim, C. T. Wearable Tactile Sensor Based on Flexible Microfluidics. *Lab Chip* **2016**, *16* (17), 3244–3250. https://doi.org/10.1039/c6lc00579a.

(96) Freund, H. J. Time Control of Hand Movements. *Prog. Brain Res.* **1986**, *64* (C), 287–294. https://doi.org/10.1016/S0079-6123(08)63423-8.

(97) Bhattacharjee, M.; Soni, M.; Escobedo, P.; Dahiya, R. PEDOT:PSS Microchannel-Based Highly Sensitive Stretchable Strain Sensor. *Adv. Electron. Mater.* **2020**, *2000445*. https://doi.org/10.1002/aelm.202000445.

(98) Lv, J.; Kong, C.; Yang, C.; Yin, L.; Jeerapan, I.; Pu, F.; Zhang, X.; Yang, S.; Yang, Z. Wearable, Stable, Highly Sensitive Hydrogel-Graphene Strain Sensors. *Beilstein J. Nanotechnol.* **2019**, *10* (1), 475–480. https://doi.org/10.3762/bjnano.10.47.

(99) Park, Y.; Chen, B.; Wood, R. J. Design and Fabrication of Soft Artificial.Pdf. **2012**, *12* (8), 2711–2718. https://doi.org/10.1093/annonc/mdx422 LK -

http://sfx.unimi.it:9003/unimi?sid=EMBASE&issn=15698041&id=doi:10.1093%2Fannonc%2Fmdx422&atitle=Cost-effectiveness+of+anti-angiogenic+agents+in+second-line+treatment+for+metastatic+colorectal+cancer.+Integrating+the+EUROPEAN+Society+for+Medical+Oncology+Magnitude+of+Clinical+Benefit+Scale+%28ESMO-MCBS%29+with+the+costs+of+drugs&stitle=Ann.+Oncol.&title=Annals+of+Oncology&volume=28&issue=&spage=vi6&epage=&aulast=Giuliani&aufirst=J.&auinit=J.&aufull=Giuliani+J.&coden=&i.

(100) Yunong Zhao, Ying Huang, Wei Hu, Xiaohui Guo, Yang Wang, Ping Liu, C. L.; Zhang, and Y. Highly Sensitive Flexible Strain Sensor Based on Threadlike Spandex Substrate Coating with Conductive Nanocomposites for Wearable Electronic Skin. *Smart Mater. Struct.* **2018**, *28*. https://doi.org/doi.org/10.1088/1361-665X/aaf3ce.

(101) Avilés, F.; Oliva-Avilés, A. I.; Cen-Puc, M. Piezoresistivity, Strain, and Damage Self-Sensing of Polymer Composites Filled with Carbon Nanostructures. *Adv. Eng. Mater.* **2018**, *20* (7), 1–23. https://doi.org/10.1002/adem.201701159.

(102) Zollo, L.; Di Pino, G.; Ciancio, A. L.; Ranieri, F.; Cordella, F.; Gentile, C.; Noce, E.; Romeo, R. A.; Dellacasa Bellingegni, A.; Vadalà, G.; Miccinilli, S.; Mioli, A.; Diaz-Balzani, L.; Bravi, M.; Hoffmann, K.-P.; Schneider, A.; Denaro, L.; Davalli, A.; Gruppioni, E.; Sacchetti, R.; Castellano, S.; Di Lazzaro, V.; Sterzi, S.; Denaro, V.; Guglielmelli, E. Restoring Tactile Sensations via Neural Interfaces for Real-Time Force-and-Slippage Closed-Loop Control of Bionic Hands. *Sci. Robot.* **2019**, *4* (27), eaau9924. https://doi.org/10.1126/scirobotics.aau9924.

(103) Qiu, A.; Li, P.; Yang, Z.; Yao, Y.; Lee, I.; Ma, J. A Path Beyond Metal and Silicon:Polymer/Nanomaterial Composites for Stretchable Strain Sensors. *Adv. Funct. Mater.* **2019**, *29* (17), 1–21. https://doi.org/10.1002/adfm.201806306.

(104) Aziz, S.; Chang, S. H. Smart-Fabric Sensor Composed of Single-Walled Carbon Nanotubes Containing Binary Polymer Composites for Health Monitoring. *Compos. Sci. Technol.* **2018**, *163*, 1–9. https://doi.org/10.1016/j.compscitech.2018.05.012.

(105) Ota, H.; Chen, K.; Lin, Y.; Kiriya, D.; Shiraki, H.; Yu, Z.; Ha, T. J.; Javey, A. Highly Deformable Liquid-State Heterojunction Sensors. *Nat. Commun.* **2014**, *5*, 1–9. https://doi.org/10.1038/ncomms6032.

(106) Tanner, J. L.; Mousadakos, D.; Giannakopoulos, K.; Skotadis, E.; Tsoukalas, D. High Strain Sensitivity Controlled by the Surface Density of Platinum Nanoparticles. *Nanotechnology* **2012**, *23* (28). https://doi.org/10.1088/0957-4484/23/28/285501.

(107) Wang, L.; Lou, Z.; Wang, K.; Zhao, S.; Yu, P.; Wei, W.; Wang, D.; Han, W.; Jiang, K.; Shen, G. Biocompatible and Biodegradable Functional Polysaccharides for Flexible Humidity Sensors. *Research* **2020**, *2020*, 1–11. https://doi.org/10.34133/2020/8716847.

(108) Muhsin Ali, Muhammad Asad Ullah Khalid, Imran Shah, Soo Wan Kim, young Su Kim, J.-H. L. and K. H. C. A Paper Based Selective and Quantitative Detection of Uric Acid Using Citrate Capped Pt Nanoparticles (PtNPs) as a Colorimetric Sensing Probe through a Simple and Remote Based Device. *New J. Chem.* **2019**. https://doi.org/10.1039/C9NJ01257E.

(109) Kubo, M.; Li, X.; Kim, C.; Hashimoto, M.; Wiley, B. J.; Ham, D.; Whitesides, G. M. Stretchable Microfluidic Radiofrequency Antennas. *Adv. Mater.* **2010**, *22* (25), 2749–2752. https://doi.org/10.1002/adma.200904201.

(110) Xu, S.; Vogt, D. M.; Hsu, W. H.; Osborne, J.; Walsh, T.; Foster, J. R.; Sullivan, S. K.; Smith, V. C.; Rousing, A. W.; Goldfield, E. C.; Wood, R. J. Biocompatible Soft Fluidic Strain and Force Sensors for Wearable Devices. *Adv. Funct. Mater.* **2019**, *29* (7), 1–14. https://doi.org/10.1002/adfm.201807058.

(111) Xu, S.; Vogt, D. M.; Hsu, W. H.; Osborne, J.; Walsh, T.; Foster, J. R.; Sullivan, S. K.; Smith, V. C.; Rousing, A. W.; Goldfield, E. C.; Wood, R. J. Biocompatible Soft Fluidic Strain and Force Sensors for Wearable Devices. *Adv. Funct. Mater.* **2019**, *29* (7). https://doi.org/10.1002/adfm.201807058.

(112) Soomro, A. M.; Jabbar, F.; Ali, M.; Lee, J.-W.; Mun, S. W.; Choi, K. H. All-Range Flexible and Biocompatible Humidity Sensor Based on Poly Lactic Glycolic Acid (PLGA) and Its Application in Human Breathing for Wearable Health Monitoring. *J. Mater. Sci. Mater. Electron.* **2019**, No. 0123456789. https://doi.org/10.1007/s10854-019-01277-1.

(113) Shintake, J.; Piskarev, E.; Jeong, S. H.; Floreano, D. Ultrastretchable Strain Sensors Using Carbon Black-Filled Elastomer Composites and Comparison of Capacitive Versus Resistive Sensors. *Adv. Mater. Technol.* **2018**, *3* (3), 1–8. https://doi.org/10.1002/admt.201700284.

(114) Anderson, A.; Menguc, Y.; Wood, R. J.; Newman, D. Development of the Polipo Pressure Sensing System for Dynamic Space-Suited Motion. *IEEE Sens. J.* **2015**, *15* (11), 6229–6237. https://doi.org/10.1109/JSEN.2015.2449304.

(115) Luo, P.; Zhuge, F.; Zhang, Q.; Chen, Y.; Lv, L.; Huang, Y.; Li, H.; Zhai, T. Doping Engineering and Functionalization of Two-Dimensional Metal Chalcogenides. *Nanoscale Horizons* **2019**, *4* (1), 26–51. https://doi.org/10.1039/c8nh00150b.

(116) Matsuzaki, R.; Tabayashi, K. Highly Stretchable, Global, and Distributed Local Strain Sensing

Line Using GaInSn Electrodes for Wearable Electronics. *Adv. Funct. Mater.* **2015**, *25* (25), 3806–3813. https://doi.org/10.1002/adfm.201501396.

(117) Muth, J. T.; Vogt, D. M.; Truby, R. L.; Mengüç, Y.; Kolesky, D. B.; Wood, R. J.; Lewis, J. A. Embedded 3D Printing of Strain Sensors within Highly Stretchable Elastomers. *Adv. Mater.* **2014**, *26* (36), 6307–6312. https://doi.org/10.1002/adma.201400334.

(118) Qi, Z.; Bian, H.; Yang, Y.; Nie, N.; Wang, F. Graphene / Glycerin Solution-Based Multifunctional Stretchable Strain Sensor with Ultra-High Stretchability , Stability , and Sensitivity. **2019**.

(119) Xu, M.; Qi, J.; Li, F.; Zhang, Y. Highly Stretchable Strain Sensors with Reduced Graphene Oxide Sensing Liquids for Wearable Electronics. *Nanoscale* **2018**, *10* (11), 5264–5271. https://doi.org/10.1039/c7nr09022f.

(120) Asplund, M.; Nyberg, T.; Inganäs, O. Electroactive Polymers for Neural Interfaces. *Polym. Chem.* **2010**, *1* (9), 1374–1391. https://doi.org/10.1039/c0py00077a.

(121) Dickey, M. D. Stretchable and Soft Electronics Using Liquid Metals. *Adv. Mater.* **2017**, *29* (27), 1–19. https://doi.org/10.1002/adma.201606425.

(122) Agaoglu, S.; Diep, P.; Martini, M.; KT, S.; Baday, M.; Araci, I. E. Ultra-Sensitive Microfluidic Wearable Strain Sensor for Intraocular Pressure Monitoring. *Lab Chip* **2018**, *18* (22), 3471–3483. https://doi.org/10.1039/c8lc00758f.

(123) Yin, F.; Yang, J.; Peng, H.; Yuan, W. Flexible and Highly Sensitive Artificial Electronic Skin Based on Graphene/Polyamide Interlocking Fabric. *J. Mater. Chem. C* **2018**, *6* (25), 6840–6846. https://doi.org/10.1039/c8tc00839f.

(124) Arain, Z.; Liu, C.; Ren, Y.; Yang, Y.; Mateen, M.; Liu, X.; Ding, Y.; Ali, Z.; Liu, X.; Dai, S.; Hayat, T.; Alsaedi, A. Low-Temperature Annealed Perovskite Films: A Trade-Off between Fast and Retarded Crystallization via Solvent Engineering. *ACS Appl. Mater. Interfaces* **2019**, acsami.9b02297. https://doi.org/10.1021/acsami.9b02297.

(125) Surmann, P.; Zeyat, H. Voltammetric Analysis Using a Self-Renewable Non-Mercury Electrode. *Anal. Bioanal. Chem.* **2005**, *383* (6), 1009–1013. https://doi.org/10.1007/s00216-005-0069-7.

(126) Khan, S. A.; Rahimoon, A. Q.; Abro, A.; Ali, M.; Hussain, I.; Ahmed, F. Electrode-Based Triboelectric Nanogenerator. *2019 2nd Int. Conf. Comput. Math. Eng. Technol.* **2019**, 1–5.

(127) Chossat, J. B.; Park, Y. L.; Wood, R. J.; Duchaine, V. A Soft Strain Sensor Based on Ionic and Metal Liquids. *IEEE Sens. J.* **2013**, *13* (9), 3405–3414. https://doi.org/10.1109/JSEN.2013.2263797.

(128) Yap, L. W.; Shi, Q.; Gong, S.; Wang, Y.; Chen, Y.; Zhu, C.; Gu, Z.; Suzuki, K.; Zhu, Y.; Cheng, W. Bifunctional Fe <inf>3</Inf>O <inf>4</Inf>@AuNWs Particle as Wearable Bending and Strain Sensor. *Inorg. Chem. Commun.* **2019**, *104* (March), 98–104. https://doi.org/10.1016/j.inoche.2019.03.020.

(129) Cheung, Y. N.; Zhu, Y.; Cheng, C. H.; Chao, C.; Leung, W. W. F. A Novel Fluidic Strain Sensor for Large Strain Measurement. *Sensors Actuators, A Phys.* **2008**, *147* (2), 401–408. https://doi.org/10.1016/j.sna.2008.05.013.

(130) Yang, Y.; Li, D.; Shen, Y. Inchworm-Inspired Soft Robot With Light-Actuated Locomotion. *IEEE Robot. Autom. Lett.* **2019**, *4* (2), 1647–1652. https://doi.org/10.1109/lra.2019.2896917.

(131) Lee, J. W.; Soomro, A. M.; Waqas, M.; Khalid, M. A. U.; Choi, K. H. A Highly Efficient Surface Modified Separator Fabricated with Atmospheric Atomic Layer Deposition for High Temperature Lithium Ion Batteries. *Int. J. Energy Res.* **2020**, *44* (8), 7035–7046. https://doi.org/10.1002/er.5371.

(132) Keulemans, G.; Pelgrims, P.; Bakula, M.; Ceyssens, F.; Puers, R. An Ionic Liquid Based Strain Sensor for Large Displacements. *Procedia Eng.* **2014**, *87*, 1123–1126. https://doi.org/10.1016/j.proeng.2014.11.362.

(133) Arabagi, V.; Felfoul, O.; Gosline, A. H.; Wood, R. J.; Dupont, P. E. Biocompatible Pressure Sensing Skins for Minimally Invasive Surgical Instruments. *IEEE Sens. J.* **2016**, *16* (5), 1294–1303. https://doi.org/10.1109/JSEN.2015.2498481.

(134) Michaud, H. O.; Dejace, L.; De Mulatier, S.; Lacour, S. P. Design and Functional Evaluation of an Epidermal Strain Sensing System for Hand Tracking. *IEEE Int. Conf. Intell. Robot. Syst.* **2016**, *2016-Novem*, 3186–3191. https://doi.org/10.1109/IROS.2016.7759492.

(135) Khalid, M. A. U.; Ali, M.; Soomro, A. M.; Kim, S. W.; Kim, H. B.; Lee, B. G.; Choi, K. H. A Highly Sensitive Biodegradable Pressure Sensor Based on Nanofibrous Dielectric. *Sensors Actuators, A Phys.* **2019**, *294*, 140–147. https://doi.org/10.1016/j.sna.2019.05.021.

(136) Xie, W.; Liu, W.; Dang, Y.; Peng, Y. Multi-scale Modelling of the Tensile Behavior of Lithium Ion Battery Cellulose Separator. *Polym. Int.* **2019**, pi.5823. https://doi.org/10.1002/pi.5823.

(137) Gottwald, M.; Herzog, H.; von der Emde, G. A Bio-Inspired Electric Camera for Short-Range Object Inspection in Murky Waters. *Bioinspir. Biomim.* **2019**, *14* (3), 035002. https://doi.org/10.1088/1748-3190/ab08a6.

(138) Zhang, L. M.; He, Y.; Cheng, S.; Sheng, H.; Dai, K.; Zheng, W. J.; Wang, M. X.; Chen, Z. S.; Chen,

Y. M.; Suo, Z. Self-Healing, Adhesive, and Highly Stretchable Ionogel as a Strain Sensor for Extremely Large Deformation. *Small* **2019**, *1804651*, 1804651. https://doi.org/10.1002/smll.201804651.

(139) Zhou, T.; Guo, B.; Xu, J. Highly Filled Glycerol/Graphite Suspensions as Fluidic Soft Sensors and Their Responsive Mechanism to Shear. *Adv. Mater. Technol.* **2020**, *2000508*, 1–10. https://doi.org/10.1002/admt.202000508.

(140) Park, S.; Ahn, S.; Sun, J.; Bhatia, D.; Choi, D.; Yang, K. S.; Bae, J.; Park, J. J. Highly Bendable and Rotational Textile Structure with Prestrained Conductive Sewing Pattern for Human Joint Monitoring. *Adv. Funct. Mater.* **2019**, *29* (10), 1–12. https://doi.org/10.1002/adfm.201808369.

(141) Wu, G.; Wu, X.; Xu, Y.; Cheng, H.; Meng, J.; Yu, Q.; Shi, X.; Zhang, K.; Chen, W.; Chen, S. High-Performance Hierarchical Black-Phosphorous-Based Soft Electrochemical Actuators in Bioinspired Applications. *Adv. Mater.* **2019**, *1806492*, 1806492. https://doi.org/10.1002/adma.201806492.

(142) Nakamura, A.; Hamanishi, T.; Kawakami, S.; Takeda, M. A Piezo-Resistive Graphene Strain Sensor with a Hollow Cylindrical Geometry. *Mater. Sci. Eng. B Solid-State Mater. Adv. Technol.* **2017**, *219*, 20–27. https://doi.org/10.1016/j.mseb.2017.02.012.

(143) Gul, J. Z.; Sajid, M.; Choi, K. H. 3D Printed Highly Flexible Strain Sensor Based on TPU-Graphene Composite for Feedback of High Speed Robotic Applications. *J. Mater. Chem. C* **2019**. https://doi.org/10.1039/c8tc03423k.

(144) Luan, J.; Wang, Q.; Zheng, X.; Li, Y.; Wang, N. Flexible Metal / Polymer Composite Films Embedded with Silver Nanowires as a Stretchable and Conductive Strain Sensor for Human Motion Monitoring. **2019**.

(145) Huang, Y.; Zhao, Y.; Pan, W.; Zhang, Y.; Guo, X.; Mao, L.; Liu, P.; Gao, L. Highly Stretchable Strain Sensor Based on SWCNTs/CB Synergistic Conductive Network for Wearable Human-Activity Monitoring and Recognition. *Smart Mater. Struct.* **2017**, *26* (9), 095017. https://doi.org/10.1088/1361-665x/aa79c3.

(146) Zhu, S.; So, J. H.; Mays, R.; Desai, S.; Barnes, W. R.; Pourdeyhimi, B.; Dickey, M. D. Ultrastretchable Fibers with Metallic Conductivity Using a Liquid Metal Alloy Core. *Adv. Funct. Mater.* **2013**, *23* (18), 2308–2314. https://doi.org/10.1002/adfm.201202405.

(147) Shi, X.; Cheng, C. H.; Zheng, Y.; Wai, P. K. A. An EGaIn-Based Flexible Piezoresistive Shear and Normal Force Sensor with Hysteresis Analysis in Normal Force Direction. *J. Micromechanics*

Microengineering **2016**, *26* (10). https://doi.org/10.1088/0960-1317/26/10/105020.

(148) Hassan, G.; Bae, J.; Hassan, A.; Ali, S.; Lee, C. H.; Choi, Y. Ink-Jet Printed Stretchable Strain Sensor Based on Graphene/ZnO Composite on Micro-Random Ridged PDMS Substrate. *Compos. Part A Appl. Sci. Manuf.* **2018**, *107* (February), 519–528. https://doi.org/10.1016/j.compositesa.2018.01.031.

(149) Zhang, S. H.; Wang, F. X.; Li, J. J.; Peng, H. D.; Yan, J. H.; Pan, G. B. Wearable Wide-Range Strain Sensors Based on Ionic Liquids and Monitoring of Human Activities. *Sensors (Switzerland)* **2017**, *17* (11), 1–10. https://doi.org/10.3390/s17112621.

(150) Lee, C. H.; Jeong, Y. S.; Ashraf, H. Cylindrical Cavity Sensor for Distinction of Various Driveability Index Gasoline with Temperature Robustness. *Sensors (Switzerland)* **2019**, *19* (21). https://doi.org/10.3390/s19214626.